

AD-A145 751

MAGNETOSPHERIC PLASMA STUDIES USING DATA FROM THE  
DYNAMICS HIGH AND LOW A. (U) SOUTHWEST RESEARCH INST  
SAN ANTONIO TX J N BARFIELD 15 MAY 84 SWRI-15-7053-2

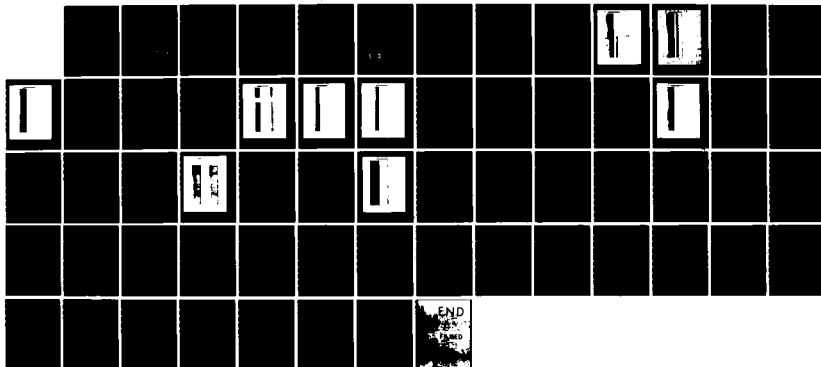
1/1

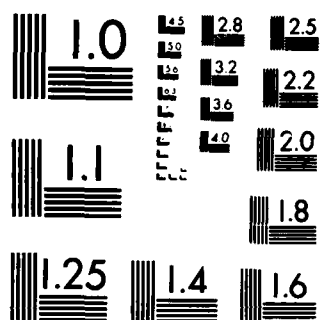
UNCLASSIFIED

AFGL-TR-84-0136 F19628-02-K-0024

F/G 4/1

NL





MICROCOPY RESOLUTION TEST CHART  
NATIONAL BUREAU OF STANDARDS-1963-A

12

AFGL-TR-84-0136

MAGNETOSPHERIC PLASMA STUDIES USING DATA FROM  
THE DYNAMICS HIGH AND LOW ALTITUDE PLASMA  
INSTRUMENTS

J. N. Barfield

Southwest Research Institute  
P. O. Drawer 28510  
San Antonio, Texas 78284

15 May 1984

Scientific Report No. 2

Approved for public release; distribution unlimited

AIR FORCE GEOPHYSICS LABORATORY  
AIR FORCE SYSTEMS COMMAND  
UNITED STATES AIR FORCE  
HANSCOM AFB, MASSACHUSETTS 01731

DTIC  
ELECTE  
SEP 21 1984  
Bgc

9 09 21 007

AD-A145 751

DTIC FILE COPY


This report has been reviewed by the ESD Public Affairs Office (PA) and is releasable to the National Technical Information Service (NTIS).

This technical report has been reviewed and is approved for publication

  
ROGER VANCOUR  
Contract Manager

  
ED MURAD  
Acting Branch Chief  
Spacecraft Interactions Br.

FOR THE COMMANDER

  
E.G. MULLEN  
Acting Division Director  
Space Physics Division

Qualified requestors may obtain additional copies from the Defense Technical Information Center. All others should apply to the National Technical Information Service.

If your address has changed, or if you wish to be removed from the mailing list, or if the addressee is no longer employed by your organization, please notify AFGL/DAA, Hanscom AFB, MA 01731. This will assist us in maintaining a current mailing list.

Do not return copies of this report unless contractual obligations or notices on a specific document requires that it be returned.

UNCLASSIFIED

SECURITY CLASSIFICATION OF THIS PAGE (When Data Entered)

REPORT DOCUMENTATION PAGE		READ INSTRUCTIONS BEFORE COMPLETING FORM
1. REPORT NUMBER AFGL-TR-84-0136	2. GOVT ACCESSION NO. AD-A145751	3. RECIPIENT'S CATALOG NUMBER
4. TITLE (and Subtitle) Magnetospheric Plasma Studies using Data from the Dynamics High and Low Altitude Plasma Instruments		5. TYPE OF REPORT & PERIOD COVERED Scientific Report No. 2
		6. PERFORMING ORG. REPORT NUMBER 15-7053-2
7. AUTHOR(s) J. N. Barfield		8. CONTRACT OR GRANT NUMBER(s) F19628-82-K-0024
9. PERFORMING ORGANIZATION NAME AND ADDRESS Southwest Research Institute P. O. Drawer 28510 San Antonio, TX 78284		10. PROGRAM ELEMENT, PROJECT AREA & WORK UNIT NUMBER 62101F 766110AB
11. CONTROLLING OFFICE NAME AND ADDRESS Air Force Geophysics Laboratory Hanscom AFB, MA 01731 Contract Monitor: Roger Vancour/PHK		12. REPORT DATE 15 May 1984
		13. NUMBER OF PAGES 61
14. MONITORING AGENCY NAME & ADDRESS (if different from Controlling Office)		15. SECURITY CLASS. (of this report) UNCLASSIFIED
		15a. DECLASSIFICATION DOWNGRADING SCHEDULE
16. DISTRIBUTION STATEMENT (of this Report)  Approved for public release; distribution unlimited		
17. DISTRIBUTION STATEMENT (of the abstract entered in Block 20, if different from Report)		
18. SUPPLEMENTARY NOTES		
19. KEY WORDS (Continue on reverse side if necessary and identify by block number)  Magnetosphere                      Space Plasma Ionosphere                          Environmental Specification Substorm                              Spacecraft Charging		
20. ABSTRACT (Continue on reverse side if necessary and identify by block number)  Plasma measurements made on the Dynamics Explorer 1 and 2 spacecraft are providing new information on the altitude dependence of polar-cap plasma populations, their sources, and the acceleration processes they undergo. In this study we have found that the polar-rain electron population apparently exhibits no significant altitude dependence between altitudes of a few hundred to approximately 20,000 km. This result was expected from the magnetosheath-like energy spectrum of the low-altitude polar rain.		

DD FORM 1473 JAN 73 EDITION OF 1 NOV 65 IS OBSOLETE

UNCLASSIFIED

SECURITY CLASSIFICATION OF THIS PAGE (When Data Entered)

UNCLASSIFIED

SECURITY CLASSIFICATION OF THIS PAGE(When Data Entered)

In the case of the polar wind, a significant velocity increase was theoretically predicted to occur between the two spacecraft altitudes, and this effect has been confirmed by the DE-1 plasma measurements. A major result of our study of the accelerated polar wind is its significant conic component, which indicates that the ions are heated perpendicularly as they emerge from the polar-cap ionosphere. The gradual decrease in polar-wind energy that is observed to occur from the cusp across to the nightside polar cap suggests that the perpendicular heating process, probably in cyclotron waves, is most intense near the cusp region.

Significant altitude effects are also observed in the plasmas that occupy magnetic flux tubes connected to polar-cap auroral arcs (or theta auroras). At DE-2, typical low-energy (approximately 100 eV) inverted-V electron distributions are observed. At DE-1 the electron and positive-ion distribution functions are consistent with electrostatic potential drops that are at times below the typical DE-1 altitude of 15,000 to 20,000 km and at times above these altitudes. Thus, compared to auroral-oval acceleration regions, those in the polar cap appear to be weaker and at significantly higher altitudes.

Counterstreaming electrons are observed at high altitudes ( $>1.5 R_E$ ) in the region of field-aligned current as indicated by the magnetic field data. For the counterstreaming electrons, the total current density computed from the plasma data in the energy range from 18 to 10,000 eV is generally about  $1-2 \mu A/m^2$ . For the downward current, low energy ( $18 < E < 235$  eV) electrons contribute more than 40% of the total plasma current density integrated above 18 eV. For the upward current, low energy ( $18 < E < 235$  eV) electrons contribute less than 50% of the total plasma current density integrated above 18 eV.

UNCLASSIFIED

SECURITY CLASSIFICATION OF THIS PAGE(When Data Entered)

# TABLE OF CONTENTS

	PAGE
I. INTRODUCTION	1
II. INSTRUMENTATION	2
III. OBSERVATIONS	3
A. Polar Rain	3
B. Accelerated Polar Wind	11
C. Acceleration Events	
D. Counterstreaming Electrons	25
1. Plasma Measurement	25
2. Magnetic Field Measurements	32
3. STARE Measurements	32
4. Ground Magnetograms	34
5. Computation of Current Density	37
6. Energy and Pitch Angle Distributions	39
IV. PRESENT STATUS AND FUTURE STUDIES	45
REFERENCES	51
PAPERS PRESENTED AT SCIENTIFIC MEETINGS	55
PUBLICATIONS SUPPORTED BY CONTRACT	56
PERSONNEL	57

**DTIC**  
**ELECTE**  
**S** **D**  
 SEP 21 1984  
**B**



Accession For	
NTIS GRA&I	<input checked="" type="checkbox"/>
DTIC TAB	<input type="checkbox"/>
Unannounced	<input type="checkbox"/>
Justification	
By _____	
Distribution/ _____	
Availability Codes	
Dist	Avail and/or Special
A-1	

## I. INTRODUCTION

Research performed during the second year of this contract continued to focus upon plasma processes in and near the polar cusp, and upon development of the statistical database from which a specification of the polar cap plasma environment is to be produced.

Four basic areas will be covered in this report: polar rain observations; polar wind observations; ion and electron acceleration events, produced by parallel electric fields; and observations of counterstreaming electrons in the auroral zone.



## II. INSTRUMENTATION

The DE-1 satellite was launched on August 3, 1981, into an elliptical polar orbit with an apogee of  $4.6 R_E$  geocentric and a perigee of 650 km altitude. The DE-1 High Altitude Plasma Instrument (HAPI) consists of five electrostatic analyzers mounted in a fan-shaped angular array at angles of  $45^\circ$ ,  $78^\circ$ ,  $90^\circ$ ,  $102^\circ$ , and  $135^\circ$  with respect to the spacecraft spin axis. Each analyzer makes differential measurements of positive ions and electrons over an energy per charge range of 5 eV/e to 32 keV/e. The energy stepping rate may be commanded over a range up to  $64 \text{ sec}^{-1}$ , producing three-dimensional plasma distributions at the six-second spin period of DE-1 (Burch et al., 1981).

The DE-2 satellite, launched with DE-1 on August 3, 1981, has an elliptical polar orbit at approximately  $300 \times 1000 \text{ km}$  altitude. DE-2 is three-axis stabilized, with one axis in the zenith, another perpendicular to the orbit plane, and the last completing a right-hand triad. The DE-2 Low Altitude Plasma Instrument (LAPI) consists of 15 ion and 15 electron energy/unit charge analyzers mounted on an external scan platform (Winningham et al., 1974). The detector array can be held approximately fixed ( $<1^\circ$ ) with respect to the local magnetic field vector. The plane of the sensors is in the orbital plane and thus in the local magnetic meridian plane. Two pairs of out-of-plane detectors allow for sampling near  $0^\circ$  and  $180^\circ$  pitch-angle when the magnetic field vector deviates significantly from the plane of the detector array.

### III. OBSERVATIONS

#### A. Polar Rain

Winningham and Heikkila (1974) first described polar rain, using data from the ISIS 1 satellite. Polar rain is the most common type of particle precipitation over the polar caps. This broad and relatively structureless electron precipitation can often fill the entire polar cap. The precipitating electrons typically have thermal energies on the order of 100 eV and are isotropic over the downcoming hemisphere. The energy flux carried by the particles is of the order of  $10^{-3}$  to  $10^{-2}$  erg  $\text{cm}^{-2}\text{sec}^{-1}$  (Burke, 1982). The spectral distribution of the polar rain electrons has the same shape as that of cusp electrons, but is lower in intensity, suggesting that polar rain originates in the magnetosheath and travels to the polar ionosphere via the lobes of the magnetotail.

Figures 1a and 1b show differential energy flux from the LAPI instrument aboard DE-2 for a portion of a polar pass on day 295 (22 October) of 1981. The top panel shows data for  $8^\circ$  pitch angle electrons, and the bottom panel shows  $45^\circ$  pitch angle ion data. The upper center panel shows  $90^\circ$  and  $0^\circ$  pitch angle electron data from the GM tube. The data are coded according to the color bars at the right. Satellite ephemeris is shown at the bottom. In this particular pass, DE-2 passed through the northern polar cusp at approximately 1306-1307 UT and into the polar cap. The polar rain can be seen clearly as a bright band in the electron panel over the energy range  $\approx 60$ -600 eV. The electron flux intensity remained fairly constant in intensity until just after 1309 UT when it abruptly decreased. Notice the lack of ion fluxes over the polar cap.

Figure 2 shows line plots of the average energy, energy flux, and density of the downcoming electrons for 1306-1311 UT. These parameters are obtained by integrating distribution functions over energy from 5 eV to 20 keV. During the entire interval, the average electron energy and density remained roughly constant. The average energy was about 100 eV and the density of downcoming electrons was in the range of  $1$ - $5 \text{ cm}^{-3}$ . These values of energy and density are representative of the polar rain. After exit from the cusp at about 1307 UT, the energy flux increased very slightly toward the pole until just after 1309 UT when it decreased by approximately 50%.

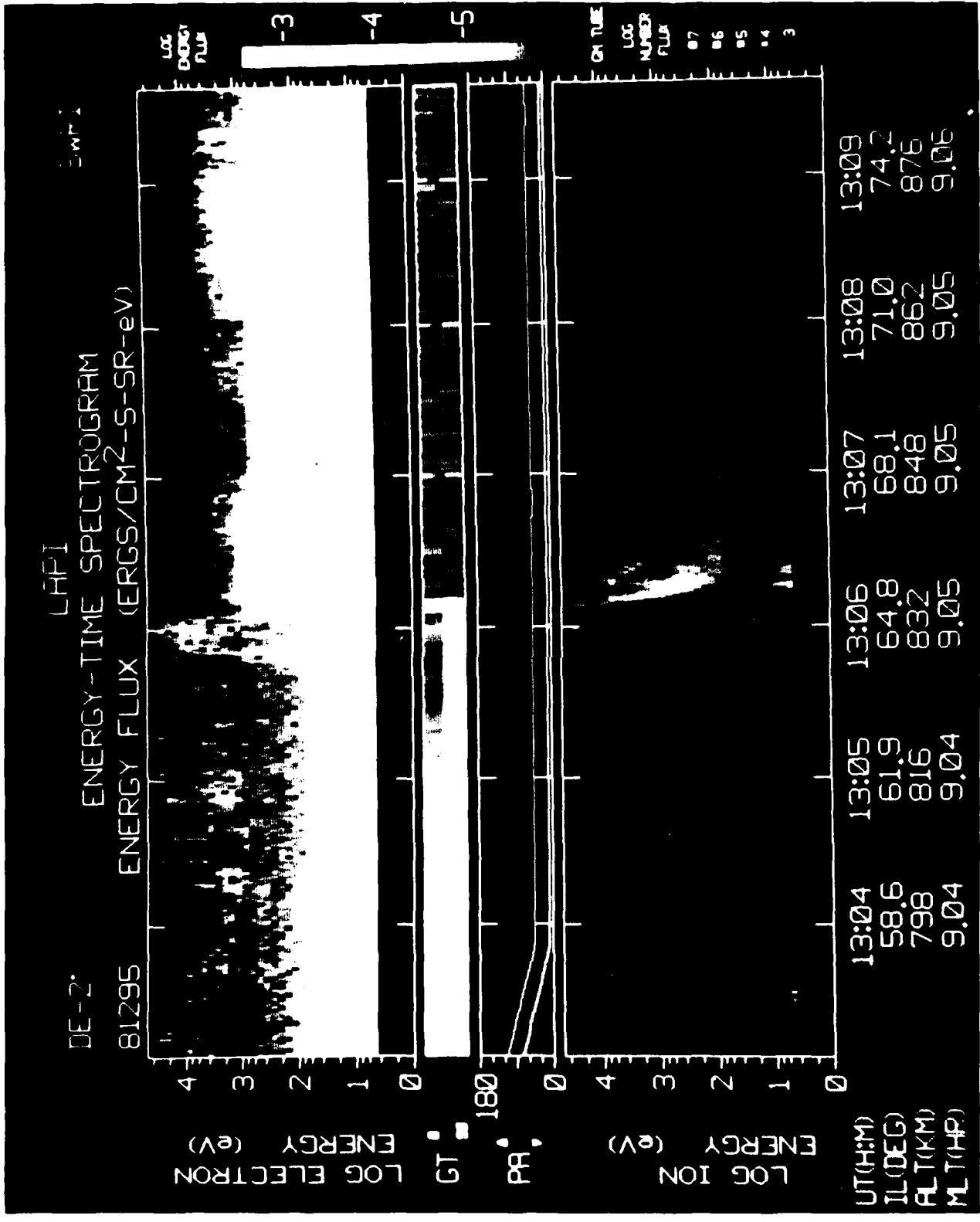


FIGURE 1a. Energy-time spectrogram of 8° pitch angle electrons and 45° pitch angle ions as observed at DE-2.

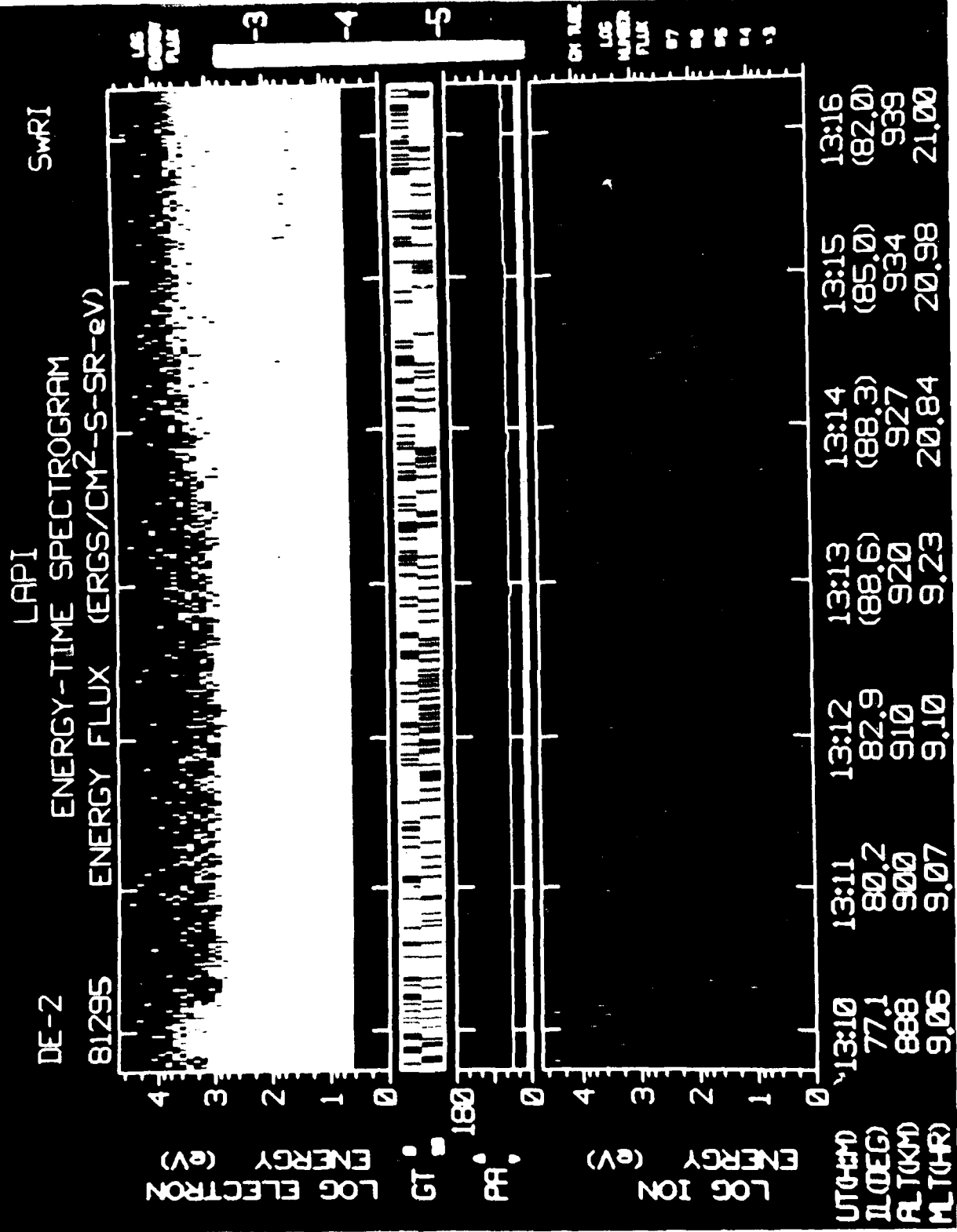


FIGURE 10. Time spectrogram of 8° pitch angle electrons and 45° pitch angle ionospheric electrons at 13:10.

# DE-2 ELECTRONS

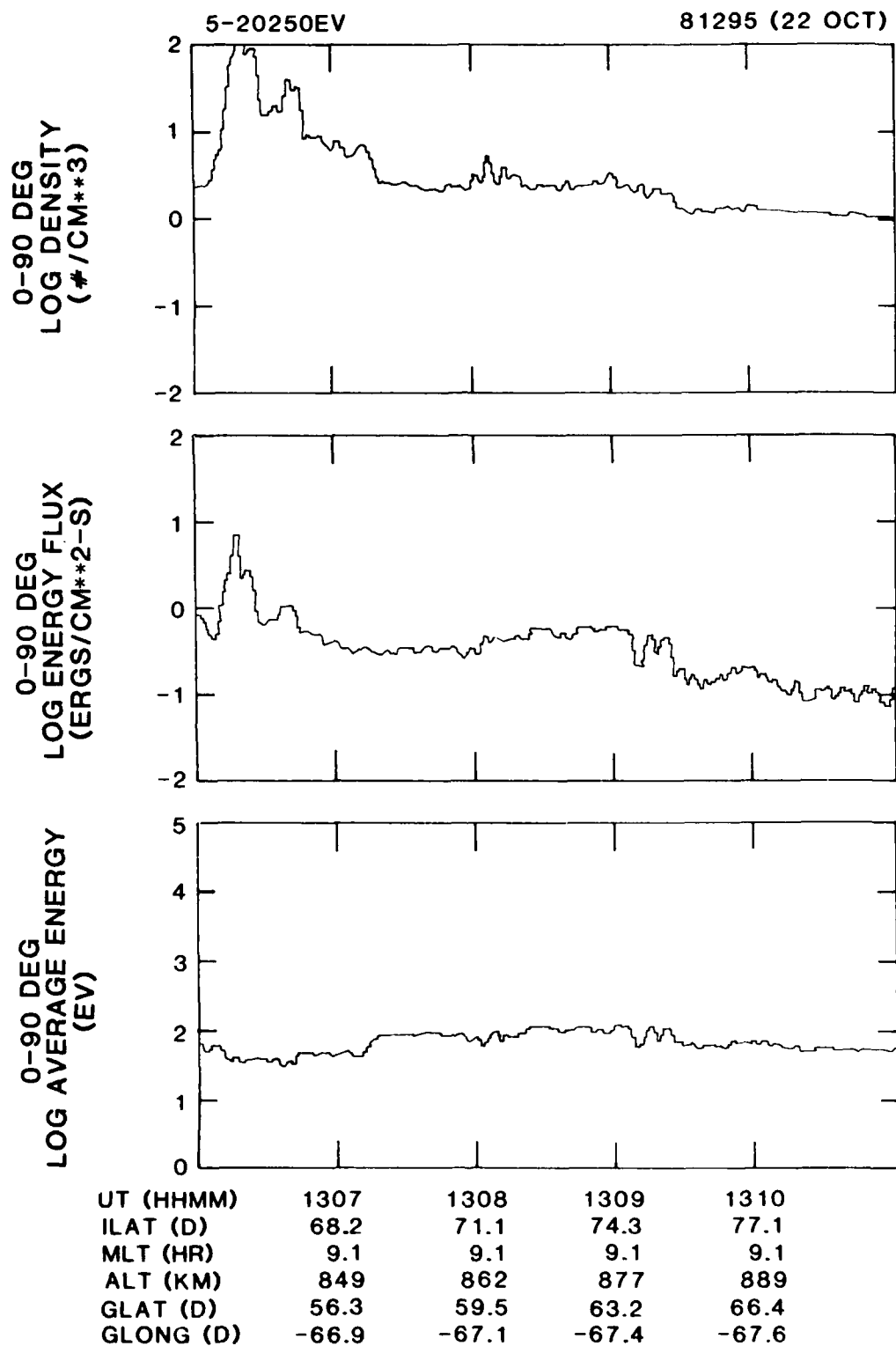


FIGURE 2. Line plots of average energy, energy flux, and density of downcoming electrons.

Figure 3 shows a DE-1 high-altitude polar pass approximately three hours after the DE-2 pass shown in Figure 1. During the interval 1617-1619 UT, DE-1 traversed the magnetic local time and invariant latitude corresponding to those of DE-2 just poleward of the cusp in Figure 1a. The format is the same as for Figure 1, except for the absence of GM tube data. The polar rain may be seen as a band in the spectrogram over the energy range  $\approx 100$ -600 eV. Bracketing the polar rain are counterstreaming energetic ( $E > 600$  eV) electron beams at  $0^\circ$  and  $180^\circ$  pitch angle and upward-moving low-energy ( $E < 100$  eV) electron beams. The source of the energetic counterstreaming electrons is open to question and presently under study by Gurgiolo and Burch (1982). Two possibilities for the source would be reflection by a potential barrier at the magnetopause (Foster and Burrows, 1976) or direct access of solar electrons. Upstreaming ion conics may be seen in the lower panel.

Comparing Figure 1 and Figure 3, it is interesting to note that the polar rain is of the same spectral nature at both altitudes, suggesting the absence of any significant acceleration between the two satellite locations. To demonstrate further the similarity between the electrons at the two satellites, Figure 4 shows number density, energy flux, and average energy at DE-1 for the period 1614-1619 UT. The average energy was  $\approx 100$  eV, density was  $\approx 1 \text{ cm}^{-3}$  and the energy flux was  $0.8 \text{ ergs cm}^{-2}\text{s}^{-1}$ . The corresponding values at lower altitudes were  $\approx 100$  eV,  $\approx 2 \text{ cm}^{-3}$ , and  $\approx 0.8 \text{ ergs cm}^{-2}\text{s}^{-1}$ .

A detailed look at the near-field-aligned electron populations at the two satellite locations is provided in Figure 5. Shown are three data sets - two single energy sweeps from LAPI, one just at the poleward edge of the cusp and one approximately  $10^\circ$  poleward of the cusp, and a single energy sweep from HAPI at a location which maps to near the location of the first LAPI spectrum. From Figure 3, we first can see that above photoelectron energies the LAPI population can be represented by a Maxwellian, allowing the temperatures to be estimated. Near the cusp a least squares fit gives a temperature of 92 eV, while farther poleward the temperature is 99 eV. The HAPI spectrum appears well-fitted by two Maxwellians above photoelectron energies. The low-energy population has a least-squares fit temperature of 65 eV, while the higher energy population has a temperature of 141 eV.

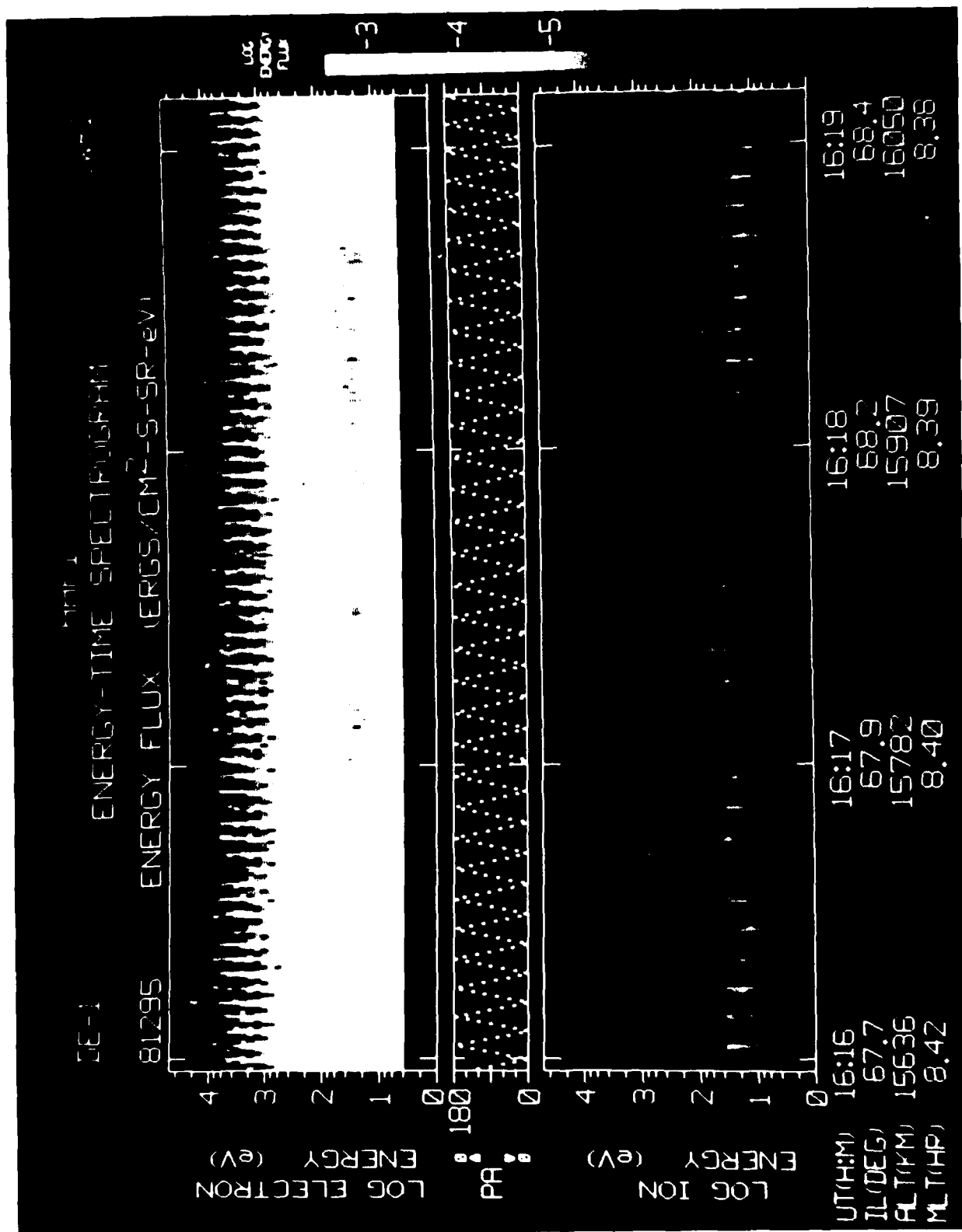


FIGURE 3. Energy-time spectrogram of electrons and ions. The detector's pitch angle is plotted in the center panel.

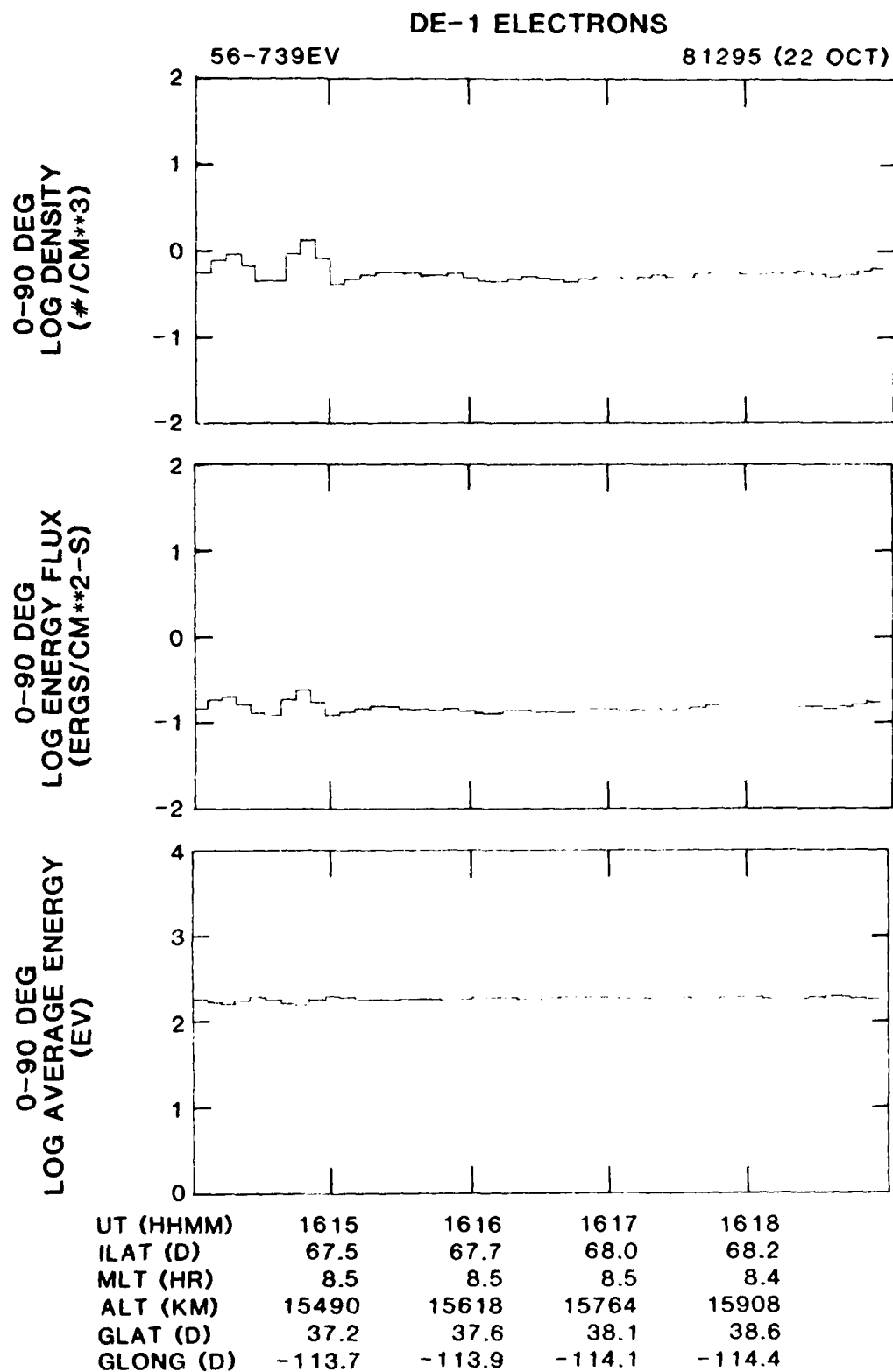


FIGURE 4. Line plots of number density, energy flux, and average energy of downcoming electrons.



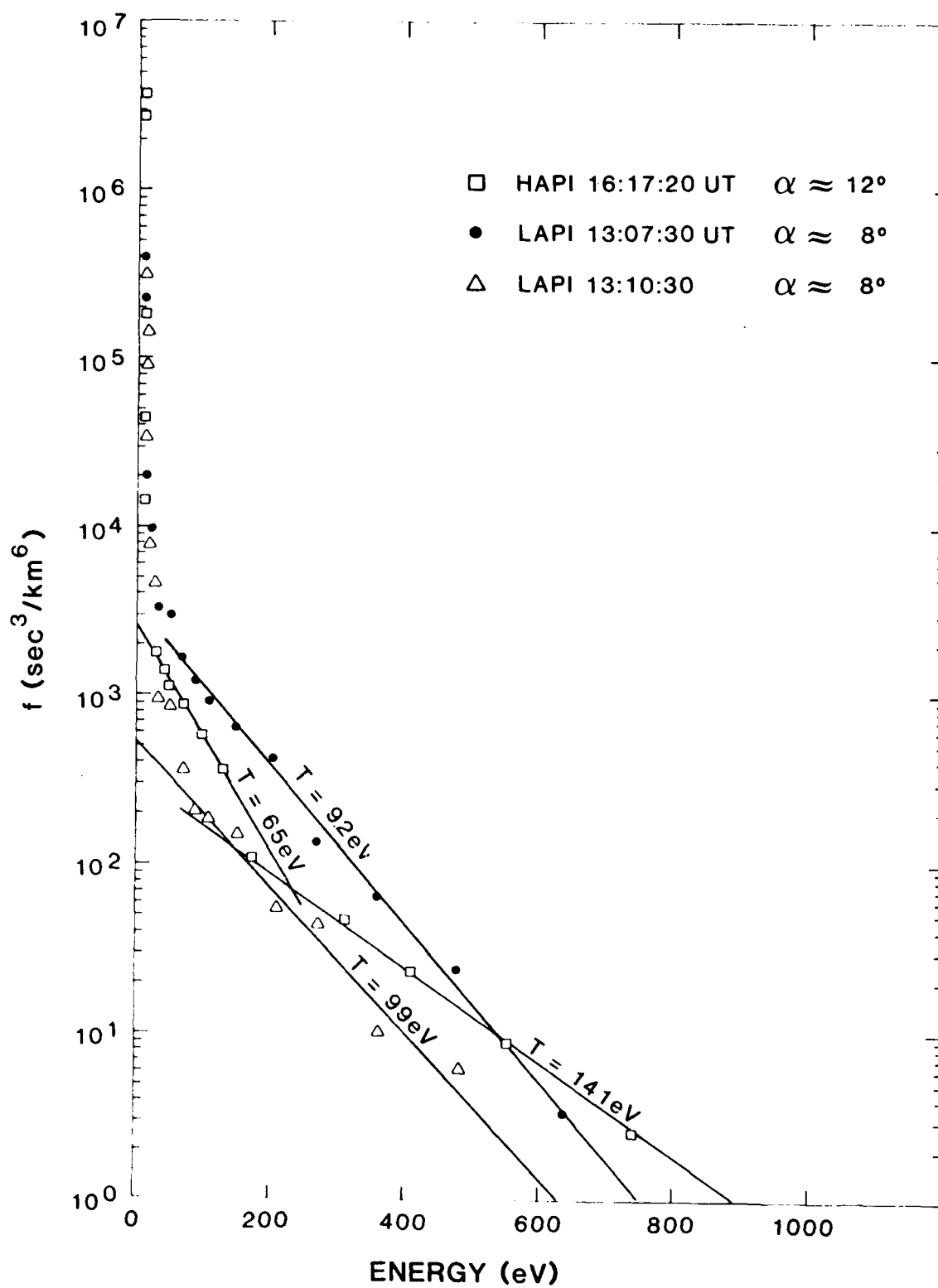


FIGURE 5. Electron energy spectra from DE-1 and DE-2 in the cusp region.

## B. Accelerated Polar Wind

The polar wind refers to the continual escape of ionospheric plasma from the polar ionosphere along open magnetic field lines. This escape of particles has consistently been observed to lead to a depletion of light ionospheric ions (ref. 7) and electrons in the upper polar ionosphere. Until recently, observations of the polar wind in the literature were limited to the low-altitude observations of Hoffman and Dodson (1980). They reported a continual upward flow of  $H^+$  and  $He^+$  over the polar caps in the range 1-5 km/sec and 1-3 km/sec, respectively. The low energy of these particles precluded most instruments from directly obtaining a distribution function. However, as pointed out by Gurgiolo and Burch (1982), polar-wind models predict that the particle velocity should increase with altitude (Schunk and Watkins, 1982). Thus, the high altitude satellite DE-1 is an ideal platform from which to study the polar wind.

Plasma data from DE-1 polar passes indicate that ions with peak differential energy fluxes in the 5 to 100 eV range are continually flowing out of the dayside cusp and polar cap. The flows have both a field-aligned and a conic component. The field-aligned component is unmistakably the polar wind. Gurgiolo and Burch (ref. 5) concluded that the conics observed in conjunction with the polar wind are polar-wind ions that have been perpendicularly heated.

The polar-wind observations to be discussed were made during a polar pass on day 272 (September 29) of 1981. Figure 6 consists of 3 sets of particle spectrograms on the same format as Figure 3. Each spectrogram displays the differential energy flux for the particle detectors which lie closest to the plane containing the local magnetic field vector.

Figure 6 shows a continuous band of upward flowing ions (near  $180^\circ$  pitch angle). The satellite was inside the cusp during the interval covered in Figure 6a. At 1411 UT, the satellite passed through the poleward cusp boundary. The upward ions showed a gradual increase in energy throughout and slightly poleward of the cusp, then they begin to decrease steadily, the peak in the differential energy flux eventually dropping below the lowest energy channel of HAPI. Within the cusp, the conic and field-aligned ions appear as "tuning forks" in the spectrograms. In the polar cap the conics become less and less apparent, as the energy and angular separation of the conic and field-aligned ions decrease. In the polar cap, there also is a shift in the field-aligned ions from  $\approx 180^\circ$  pitch angle to  $\approx 165^\circ$ , indicating an antisunward flow.

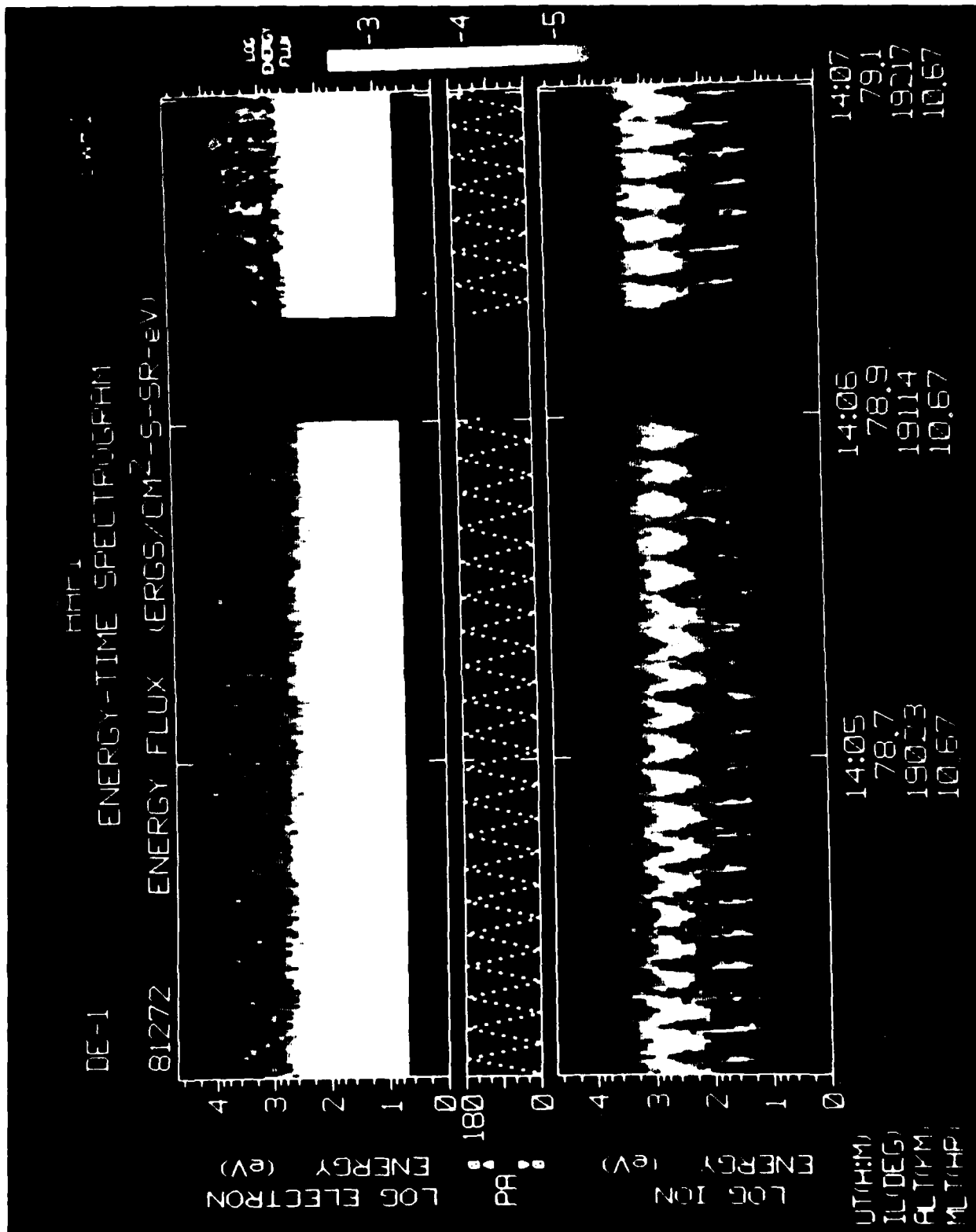


FIGURE 6a. Energy-time spectrogram using same format as Figure 3.

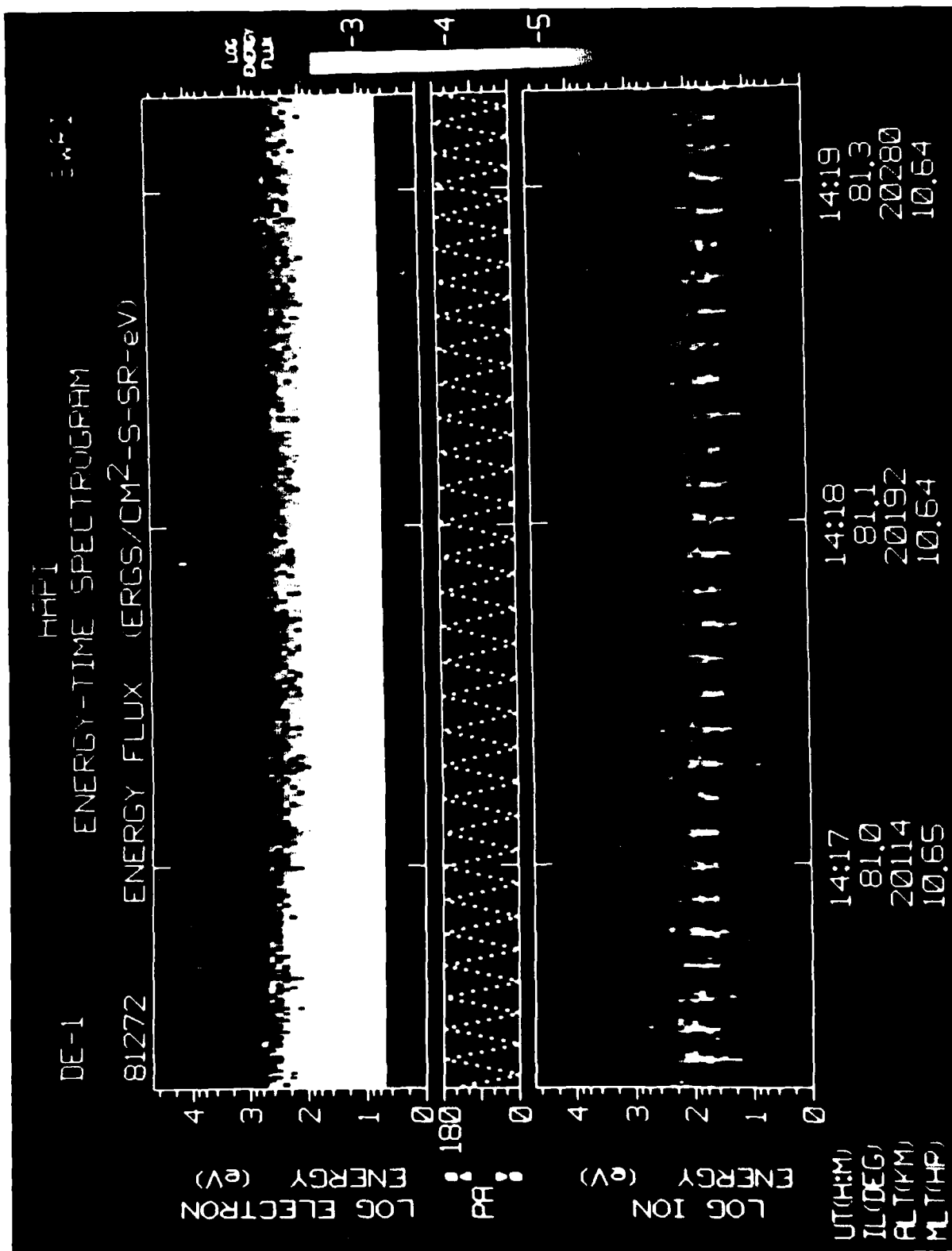


FIGURE 6b. Energy-time spectrogram using same format as Figure 3.

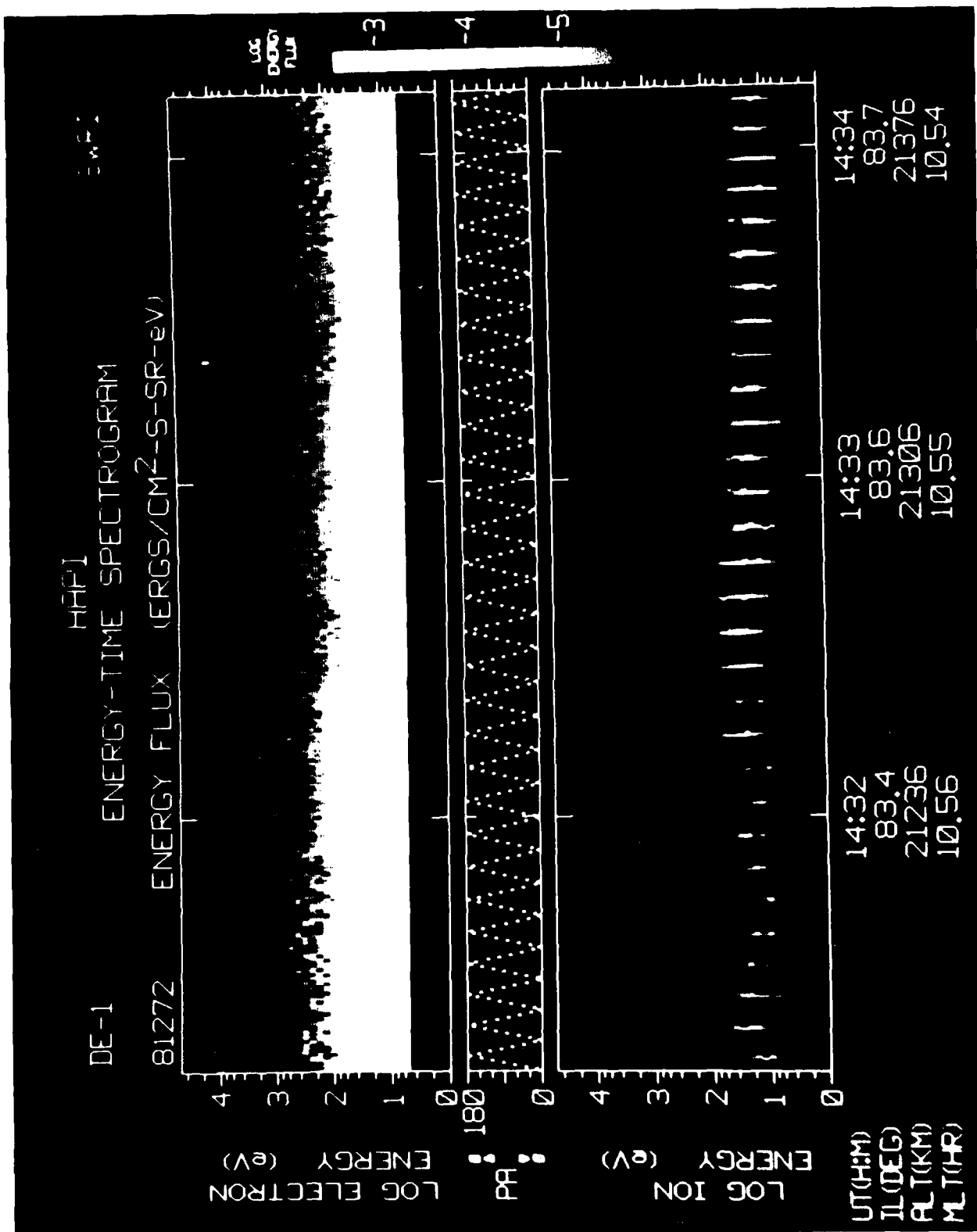


FIGURE 6c. Energy-time spectrogram using same format as Figure 3.

Figure 7 shows a detailed view of the field aligned ion population. Two data sets are shown, each of which was averaged over four satellite revolutions to improve counting statistics. Each of the distributions was transformed to the rest frame of the plasma prior to averaging (except for S/C charging which was about 20V). The two data sets were taken beginning 1434:05 UT (solid circles) and 1434:54 UT (open circles). In Figure 7 Maxwellian distributions are straight lines, with the slope being proportional to the plasma temperature and the intercept with the distribution axis being proportional to the plasma density.

From Figure 7 we can see that the field-aligned ion component observed in the polar regions is comprised of two ion populations--a low energy component with temperature below .5 eV and a high energy tail with temperature above 1.5 eV. Both ion populations would appear to be well represented by a Maxwellian distribution, allowing the estimates of the temperatures to be made. A least squares fit to the low-energy population of Figure 7 gives a temperature of  $.29 \pm .16$  eV ( $3200^\circ\text{K} \pm 1800\text{K}$ ). The corresponding temperature of the high energy plasma population in Figure 7 is found to be  $2.7 \pm .7$  eV. The peak at about 1 eV may be due to an ion heavier than  $\text{H}^+$ .

There is little doubt that the lower energy, field-aligned ions constitute the "classical" polar wind. The high energy tail, however, is not a feature predicted by polar-wind models. It is likely that this hotter plasma is the result of a perpendicular heating of polar-wind ions. Assuming that all ions in the polar wind are of equal temperature, Figure 7 gives heating on the order of 4 to 10.

We envision a scenario as shown in Figure 8 occurring during the polar wind escape along magnetic field lines. At low altitudes the generation of the polar wind occurs and ionospheric ions begin to escape along the open polar cap and cusp field lines (Figure 8a). The presence of ion perpendicular heating along the open field lines produces the characteristic conic signature (Figure 8b). The distribution above the heating region can be considered a two-component plasma consisting of unheated and heated polar-wind particles. The unheated polar wind is still field aligned, while the heated ions have large velocities in the direction perpendicular to  $\underline{B}$ . As the distribution travels upward, the perpendicular arms of the distribution will begin to collapse toward the magnetic field direction in accordance with the first adiabatic invariant, and a field-aligned high energy tail to the polar wind should

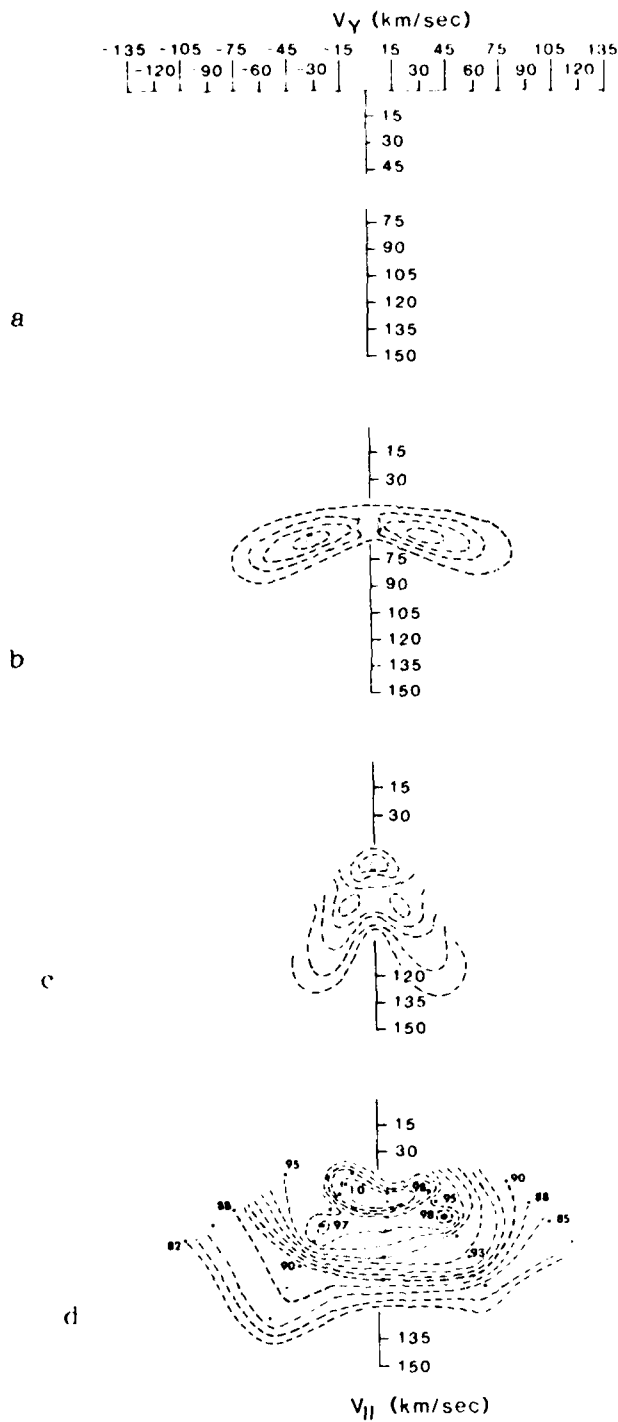


FIGURE 8. Evolution of polar wind. Shown are isocontours of the distribution function in phase space.

develop (Figure 8c). Figure 8d shows contours of a typical conic/polar-wind population measured in the cusp on day 272.

Ion conics have been reported by numerous people (Ungstrup et al., 1979; Gorney et al., 1981). Theories as to the production of the conic ion distribution have favored a perpendicular heating by electrostatic ion-cyclotron waves (Dusenberry and Lyons, 1981; Lysak et al., 1980), although recently (Chang and Coppi, 1981) it has been proposed that a heating by lower hybrid waves may also be a viable conic generation mechanism. The problem is, however, that most of these theories are applicable only at low altitudes in the auroral zone. Adaptations of the theories to the environment of the polar cap must be made to explain these observations.

Using the observed conic pitch angle distribution, the altitude of the observation and an assumed value for the initial conic pitch angle, it is possible through the first adiabatic invariant to estimate the altitude of the conic generation. In general the initial conic pitch angle for such computations is assumed to be  $90^\circ$ ; however, if the source plasma already has a significant  $V_{\parallel}$ , as the polar wind does, then the initial conic pitch angle is expected to shift to lower values. Using a dipolar magnetic field approximation and estimating the values of the initial conic pitch angle through energy conservation arguments (which assume that  $V_{\parallel}$  does not change between the observation height and the conic height) we estimate the heating to occur at an altitude of about 12,000 km--constant throughout both the cusp and polar cap. By using an initial conic pitch angle of  $90^\circ$  we can place a lower limit to the heating altitude at 8000 km.

#### C. Acceleration Events

The electrical coupling between the high-altitude and low-altitude regimes of the polar cap is an important aspect of magnetosphere-ionosphere interactions. The unique placement of the Dynamics Explorer orbits with respect to each other has afforded an excellent opportunity to investigate this coupling between the two regimes. Frequently, DE-1 and DE-2 observe signatures of field-aligned acceleration of ions and electrons above the polar cap. In this section, we briefly present observations made on October 17, 1981 (day 81290) above a "theta aurora" signature.



Figure 9 shows a spectrogram of  $180^\circ$  ions and  $0^\circ$  pitch angle electrons from HAPI. The satellite crossed the polar-cap arc field lines during the interval 1630-1650 UT. Two intervals of intense electron fluxes below 1 keV were seen:  $\approx 1631:30$ - $1633:15$  UT and  $\approx 1642$ - $1649$  UT. Figure 10 shows contour

plots of the log of the distribution functions of ions (Figure 10a) and electrons (Figure 10b) for the interval 1632:45-1632:57 UT. The ions showed a strong upgoing beam at approximately 100 eV. The electron fluxes were isotropic except for a loss cone. Thus, the combined electron and ion observations indicated that an approximately 100 eV potential drop lay below the satellite altitude.

Figure 11 shows contours in the same format as Figure 10, for the interval 1646:30 to 1646:36 UT. By this time the ions had become isotropic, while the electrons showed a downcoming beam of  $\approx 100$  eV. Thus, the acceleration region appears now to be above the satellite altitude (17313 km) while remaining at  $\approx 100$  eV.

The plasma characteristics described above are very similar to those observed by DE-1 in the high altitude ( $>15,000$  km) nightside auroral zone, except that the energy of the polar cap acceleration events is lower. Correlation studies by Hardy et al. (1982) have already noted that the plasma signatures of polar cap acceleration events at low altitudes are similar to those of evening discrete arcs. The parallel electric field responsible for the polar-cap acceleration could be produced by the same process as the evening auroral arcs.

Satellite observations of convection and electron precipitation at low altitudes ( $<1000$  km) have indicated that convective electric fields point toward the region of polar-cap acceleration ( $\nabla \cdot \mathbf{E} < 0$ ) (Burch et al., 1979). The polar cap acceleration region is therefore a region of negative space charge. Burke et al. (1982) used the simultaneous electric field, magnetic field and electron flux measurements of the S3-2 satellite to demonstrate that upward Birkeland currents were embedded in regions of polar cap acceleration. These observations suggest that field-aligned potentials develop as a result of imperfect mapping of magnetospheric convective electric fields to the ionosphere (Hardy et al., 1982; Burke et al., 1982).

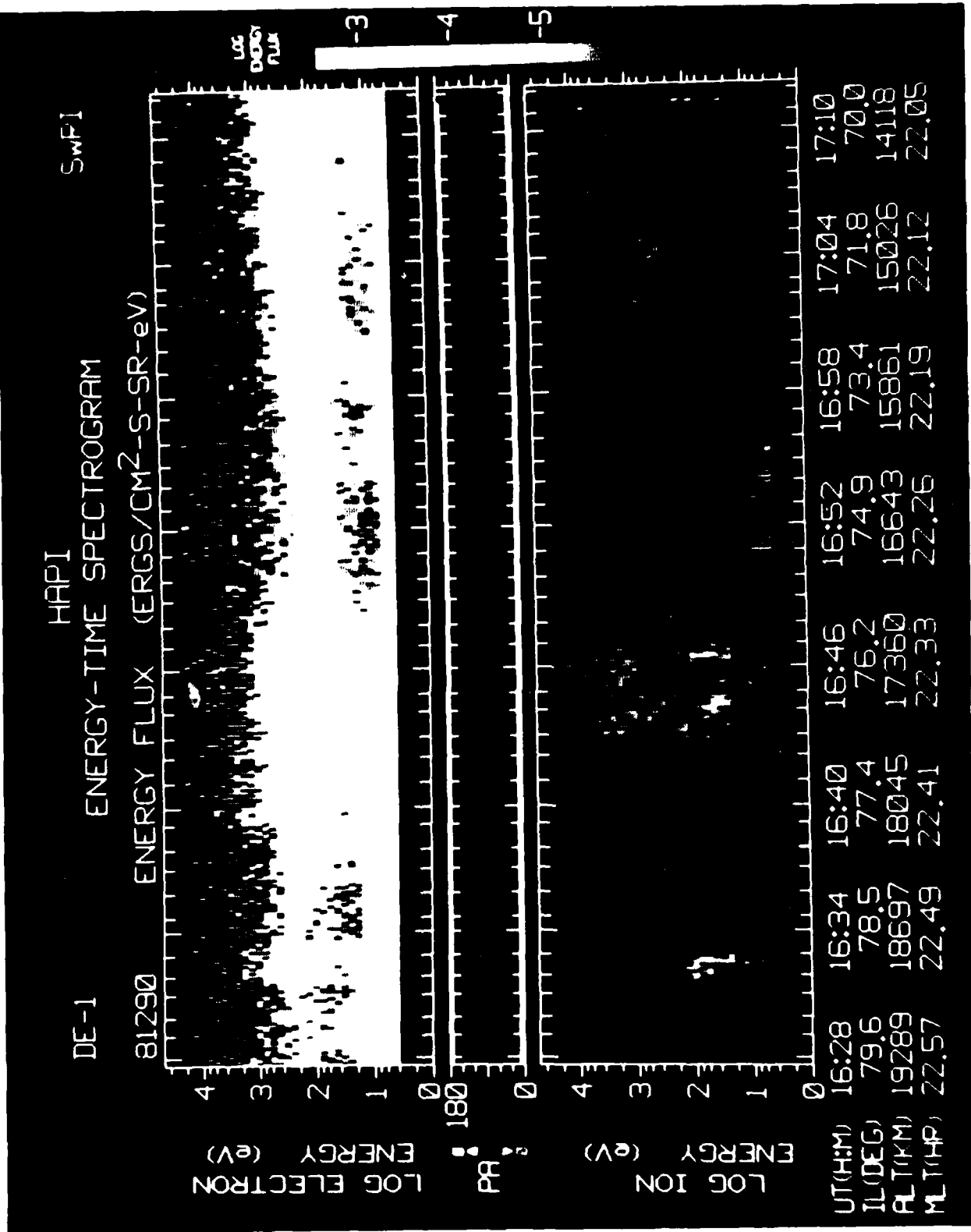
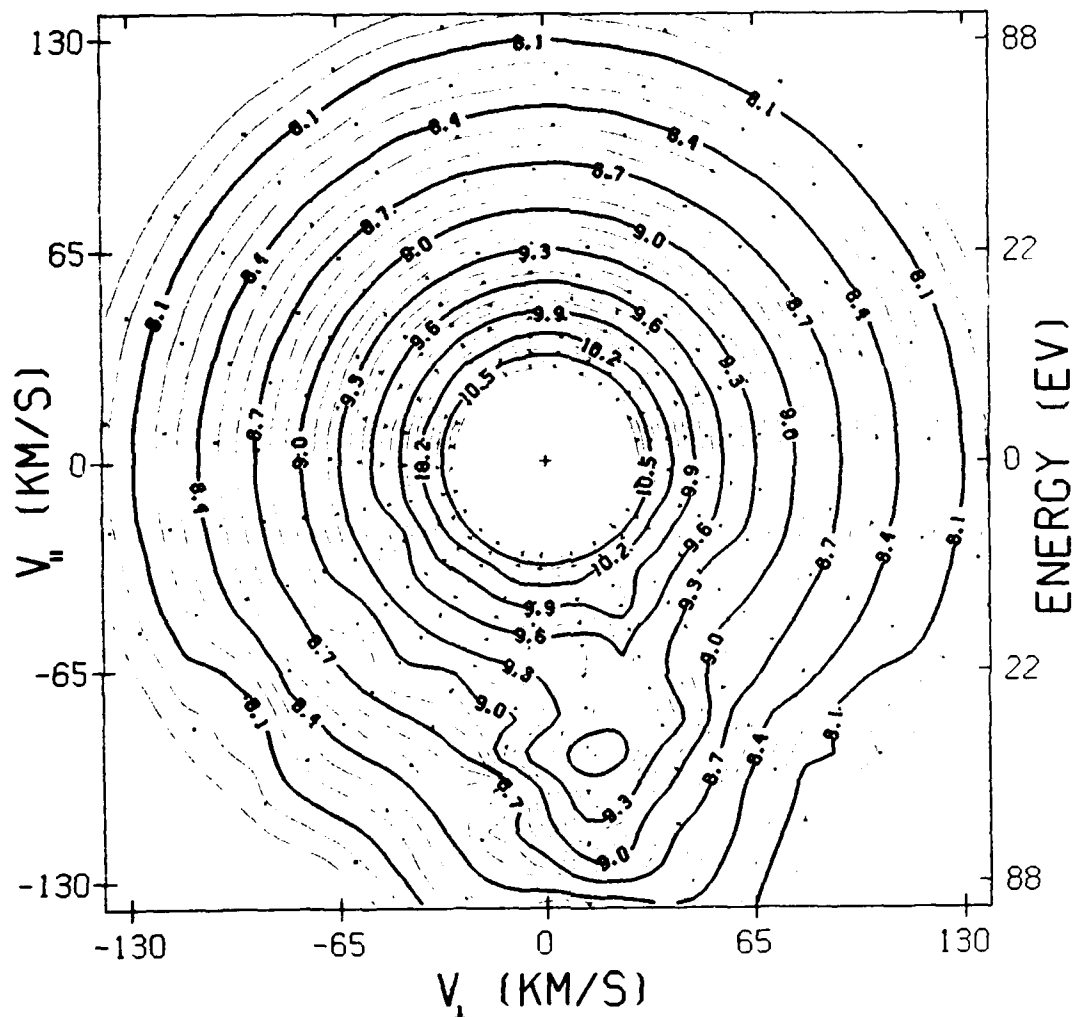


FIGURE 9. Energy-time spectrograms for 180° pitch angle ions and 0° pitch angle electrons observed at DE-1.

DE-1 HAPI IONS  
81290 (17 OCT. 81)  
16:32:45.1 TO 16:32:57.1 U.T.



DISTRIBUTION CONTOURS LOG F (SEC<sup>3</sup>/KM<sup>6</sup>)

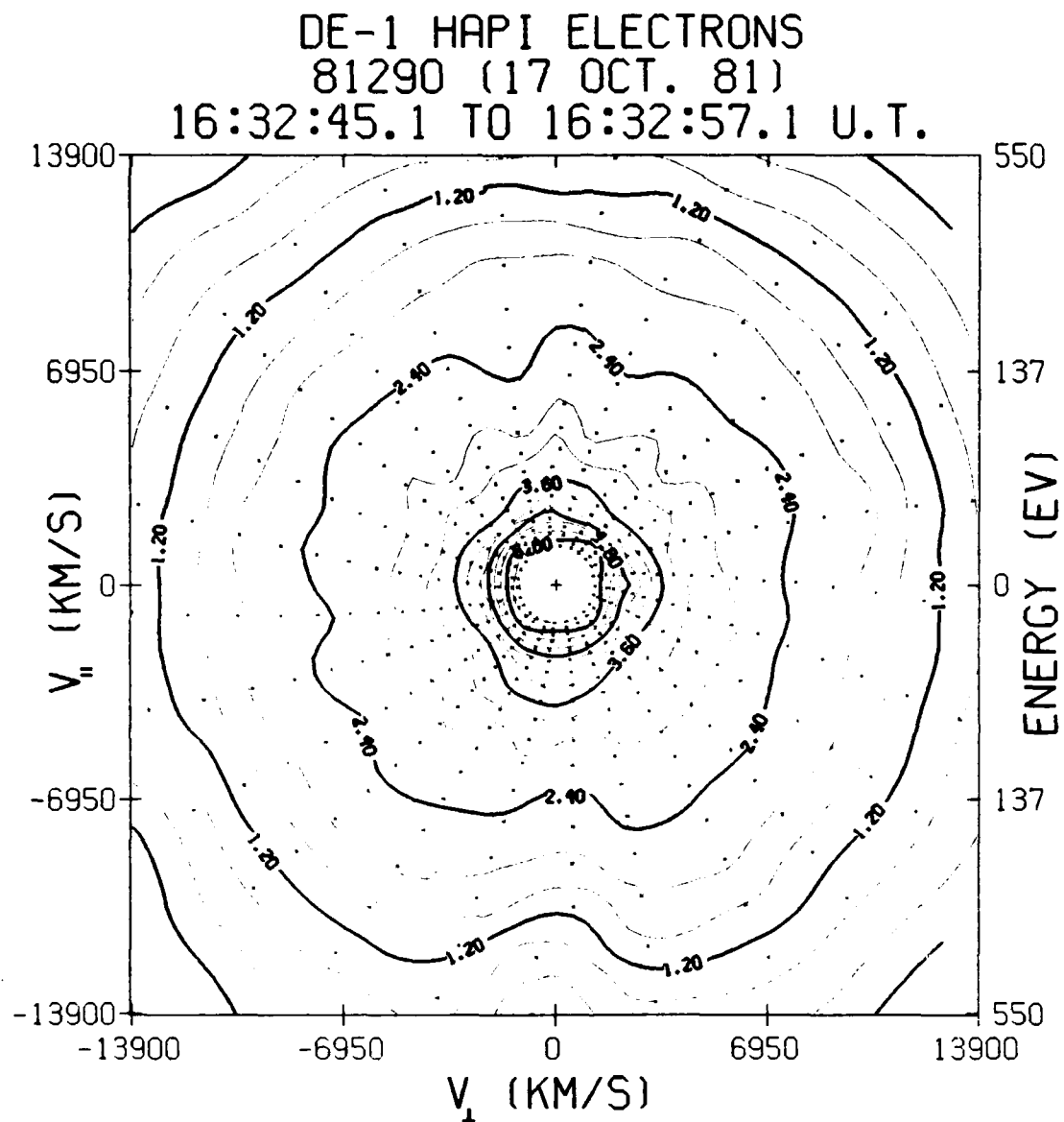
ILAT (D) 78.8  
MLT (HR) 22.6  
ALT (KM) 18819  
GLAT (D) 75.9  
GLONG (D) 66.3

MIN EV	MAX EV	AV. EV.	AMPS/M <sup>2</sup>
6.	417.	4.17E+01	-1.47E-08

FLUX (1/CM <sup>2</sup> S)	DEN (1/CM <sup>3</sup> )	ERGS/CM <sup>2</sup> S
90 - 180	90 - 180	90 - 180
1.05E+07	1.27E+00	9.59E-04

VPAR (KM/S)	PC (MMOS)	HC (MMOS)
-7.23E+01	N/A	N/A

FIGURE 10a. Isocontours of the distribution function for ions at DE 1.



ILAT (D) 78.8  
 MLT (HR) 22.6  
 ALT (KM) 18819  
 GLAT (D) 75.9  
 GLONG (D) 66.3

DISTRIBUTION CONTOURS LOG F (SEC<sup>3</sup>/KM<sup>6</sup>)

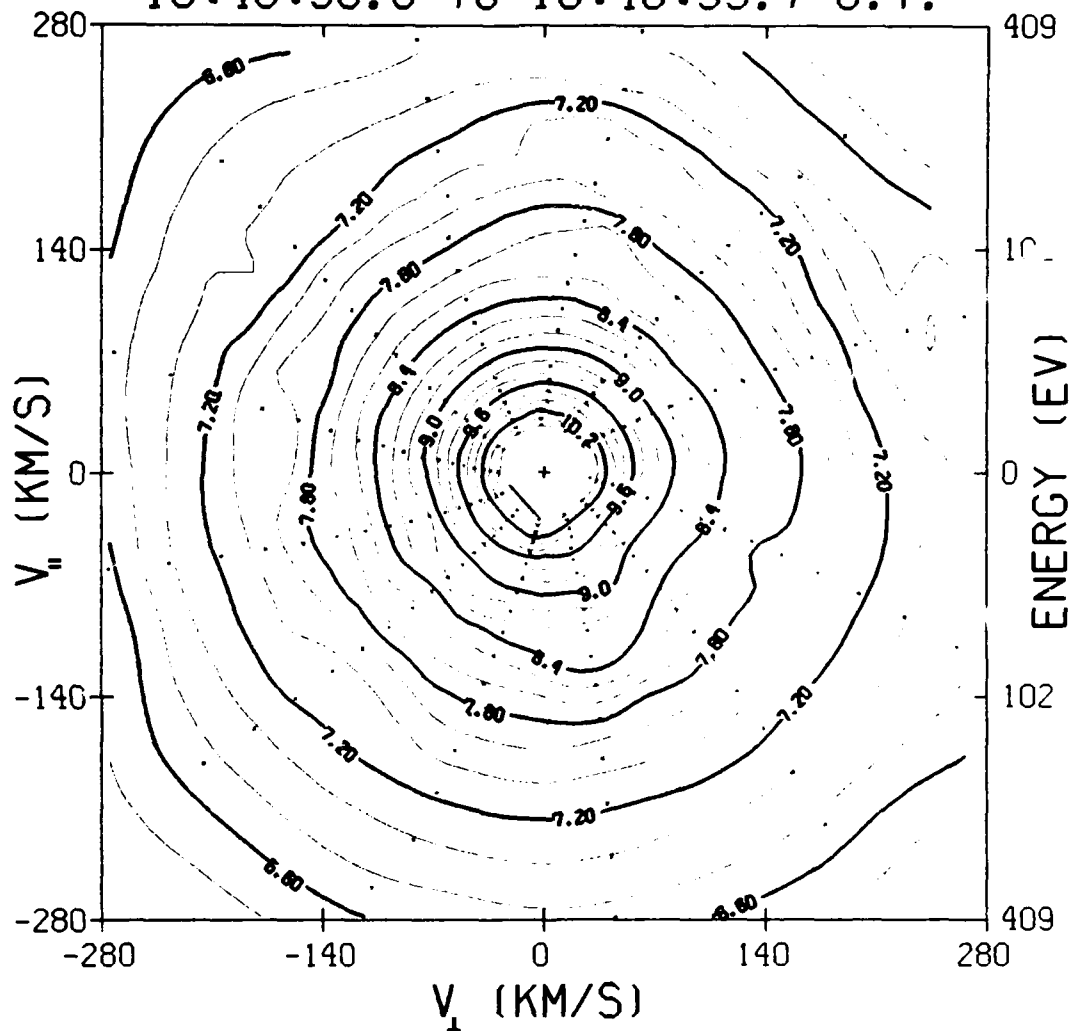
MIN EV	MAX EV	AV. EV.	AMPS/M <sup>2</sup>
6.	739.	1.60E+01	-1.47E-07

FLUX (1/CM <sup>2</sup> S)	DEN (1/CM <sup>3</sup> )	ERGS/CM <sup>2</sup> S
0 - 90	0 - 90	0 - 90
4.02E+09	2.04E+01	2.84E-01

VPAR (KM/S)	PC (MHOS)	HC (MHOS)
-2.24E+01	N/A	N/A

FIGURE 10b. Isocontours of the distribution function for electrons at DE-1.

DE-1 HAPI IONS  
81290 (17 OCT. 81)  
16:46:30.0 TO 16:46:35.7 U.T.



DISTRIBUTION CONTOURS LOG F (SEC<sup>3</sup>/KM<sup>6</sup>)

ILAT (D) 76.1  
MLT (HR) 22.4  
ALT (KM) 17313  
GLAT (D) 70.7  
GLONG (D) 63.0

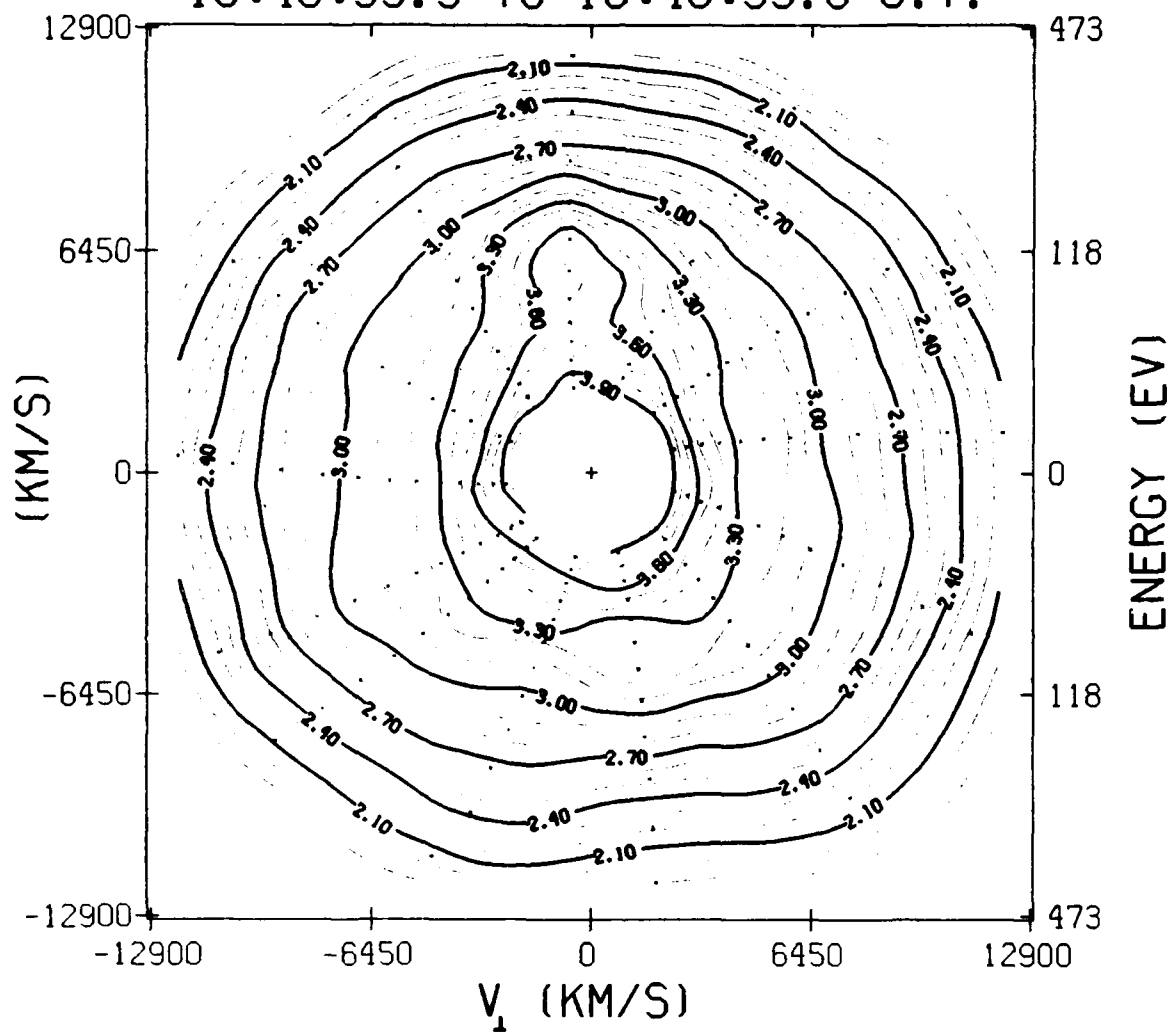
MIN EV	MAX EV	AV. EV.	AMPS/M <sup>2</sup>
6.	554.	2.91E+02	-3.77E-09

FLUX (1/CM <sup>2</sup> S)	DEN (1/CM <sup>3</sup> )	ERGS/CM <sup>2</sup> S
0 - 90	0 - 90	0 - 90
9.44E+06	4.17E-01	5.09E-03

VPAR (KM/S)	PC (MMOS)	HC (MMOS)
-1.32E+01	N/A	N/A

FIGURE 11a. Isocontours of the distribution function for ions at DE-1.

DE-1 HAPI ELECTRONS  
81290 (17 OCT. 81)  
16:46:33.3 TO 16:46:39.6 U.T.



ILAT (D) 76.1  
MLT (HR) 22.4  
ALT (KM) 17297  
GLAT (D) 70.6  
GLONG (D) 63.0

MIN_EV	MAX_EV	AV. EV.	AMPS/M <sup>2</sup>
18.	13206.	1.96E+02	6.61E-08

FLUX (/CM <sup>2</sup> S)	DEN (/CM <sup>3</sup> )	ERGS/CM <sup>2</sup> S
0 - 90	0 - 90	0 - 90
2.29E+09	3.03E+00	1.07E+00

VPAR (KM/S)	PC (MHOS)	HC (MHOS)
6.76E+01	2.063	2.908

FIGURE 11b. Isocontours of the distribution function for electrons at DE-1.

## D. Counterstreaming Electrons

### D.1 Plasma Measurement

The plasma data obtained by the High Altitude Plasma Instrument (HAPI) [Burch et al, 1981] on DE-1 are shown in Figures 12-16 for 18 September 1981 (day 261). Figure 12 is a spectrogram of electron energy fluxes for a 26-minute time interval from 2128 to 2154 UT. The top panel shows electron energy fluxes at 0° pitch angle (downward), and the bottom spectrogram shows electron energy fluxes at 90° pitch angle. The vertical scale is energy in a logarithmic scale, and the horizontal scale is UT. The energy fluxes measured at both pitch angles were enhanced after 2133 UT, indicating that DE-1 encountered a plasma injection boundary. At this time, the spacecraft was at 67° invariant latitude, 2400 (MLT) and 14,000 km altitude, and moving equatorward near the midnight meridian plane. A second enhancement of energy flux occurred after 2146 UT. The energy flux remained at high levels until the data gap at 2154 UT.

This summary spectrogram shows two distinct populations of electron fluxes. At energies around several keV are the energetic precipitating electron fluxes that are believed to originate in the plasma sheet. At lower energies, from 10 to several hundred eV, enhancements of energy fluxes were detected sporadically around 2135, 2139, and 2148 UT. These low energy electron fluxes are enhanced in the field-aligned direction because the observed energy flux was larger at 0° pitch angle (top panel) than at 90° pitch angle (bottom panel). These enhanced electron fluxes in the field-aligned direction are similar to those observed at synchronous orbit during plasma injection events [Lin et al., 1979; Moore and Arnoldy, 1982].

In Figure 13, we show the electron density and energy flux integrated from 18 eV to 10 keV over the whole pitch angle range. Before the plasma injection around 2133 UT, the number density was about  $1 \text{ cm}^{-3}$  and the integrated energy flux was about  $1 \text{ ergs/cm}^2\text{-s}$ . After the injection, the number density increased to about  $10 \text{ cm}^{-3}$  and the integrated energy flux increased to  $10 \text{ ergs/cm}^2\text{-s}$ . Electrons with energy less than 1 keV contributed about 10% of the integrated energy flux and about 70% of the number density. Around 2148 UT, the integrated energy flux reached a peak value exceeding  $100 \text{ ergs/cm}^2\text{-s}$ . We found this plasma injection event to be the most intense in the HAPI data that have been processed so far. The three-hour Kp index during this time was 6-.

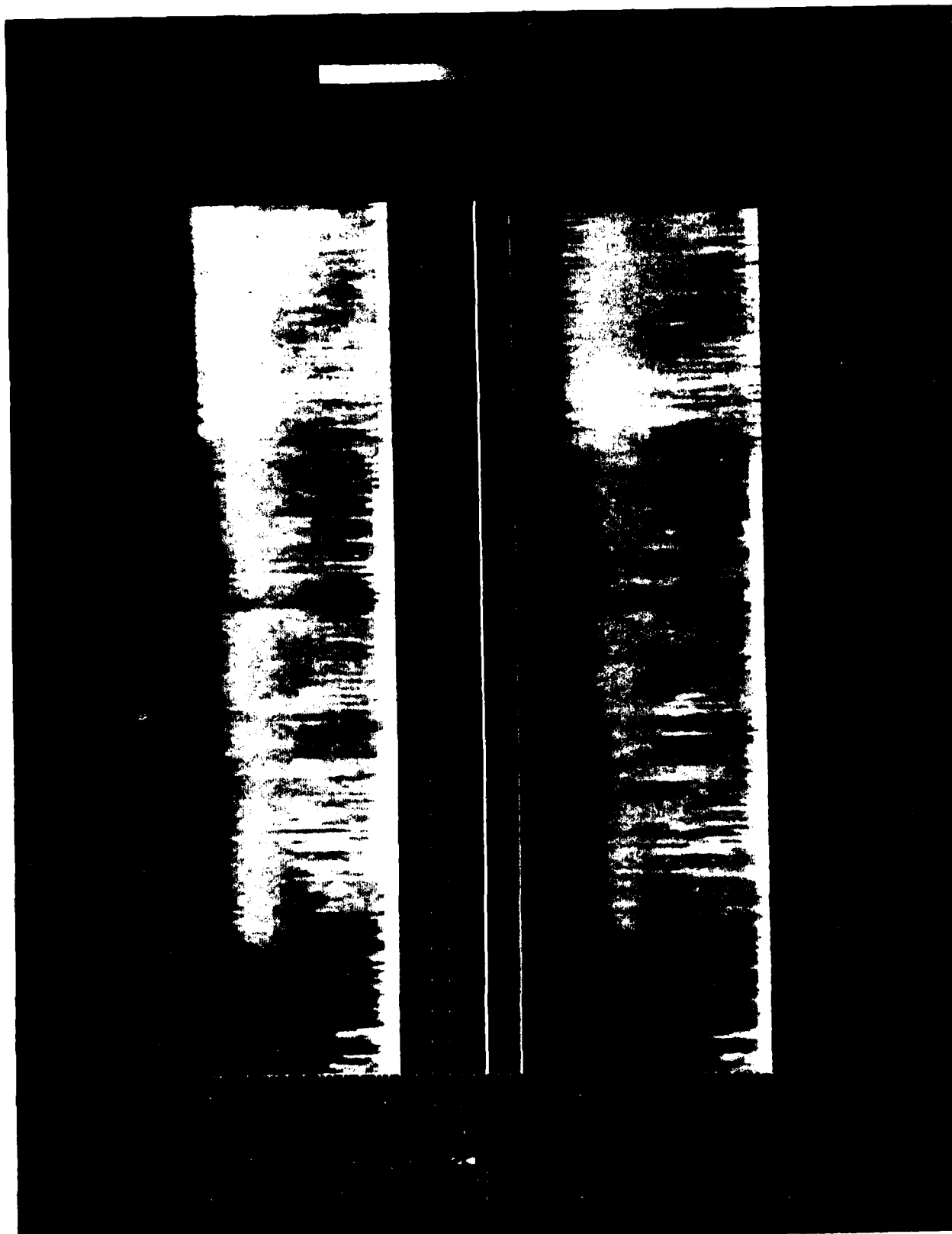


FIGURE 12. Energy-time spectrograms of electron energy fluxes at 0° pitch angle (top) and 90° pitch angle (bottom).



# DE-1 ELECTRONS

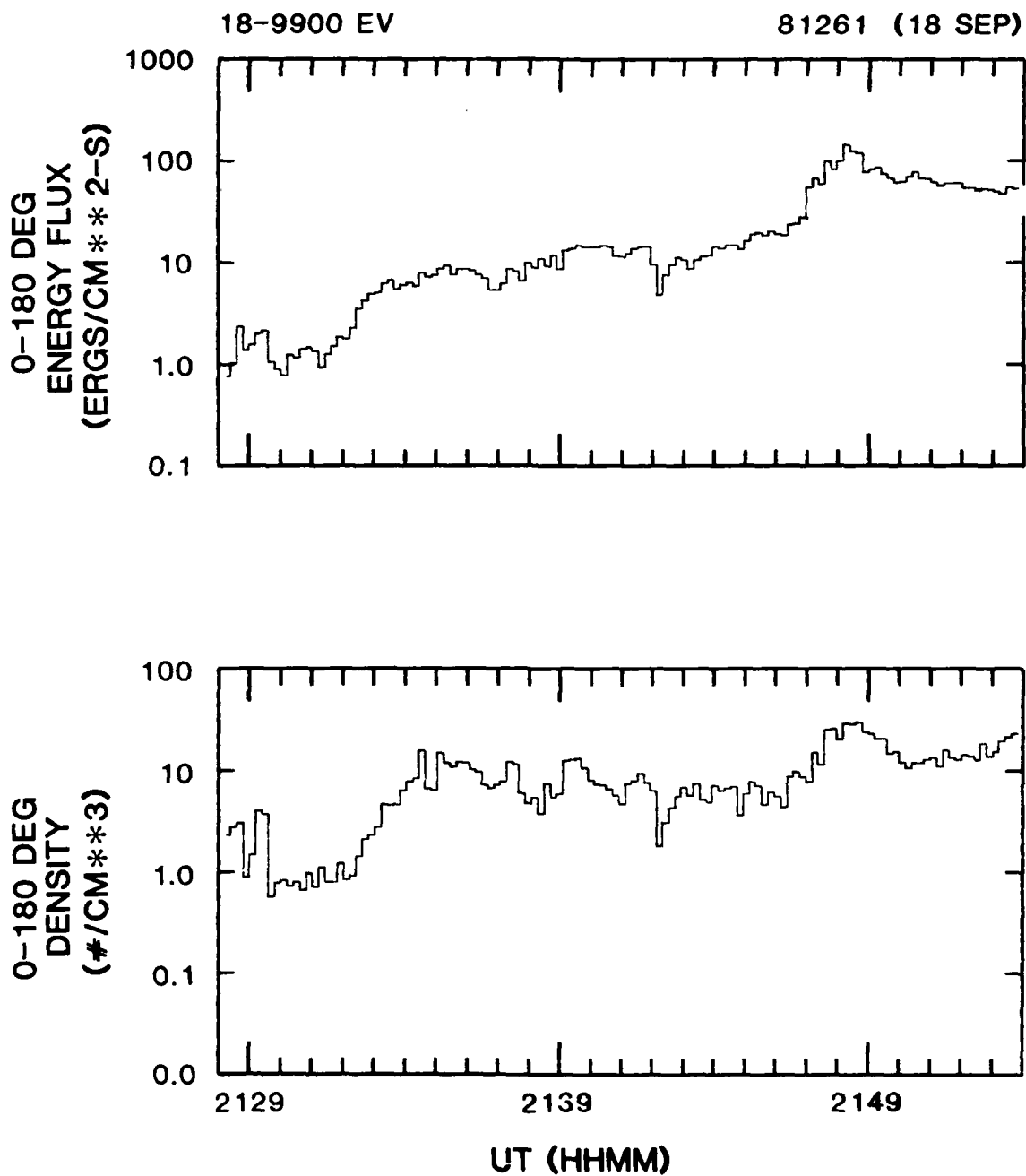


FIGURE 13. Number density and total energy flux integrated from 18 to 10,000 eV over the whole pitch angle range.

The electron and ion energy fluxes for the full pitch angle range ( $0^\circ$ - $180^\circ$ ) are presented in Figure 14 for one counterstreaming electron event during 2147-2150 UT. The DE-1 altitude in this time interval was about 11400 km. The energy fluxes shown are spin-modulated with a period of 6 seconds. The electron spectrogram (top panel) shows bright vertical stripes below 1 keV, indicating an enhancement of energy flux in that energy range. The center panel, which displays the detector pitch angle, shows that the detector measured enhanced energy fluxes only near  $0^\circ$  and  $180^\circ$ . Hence the measured low energy ( $<1$  keV) electrons were counterstreaming along field lines. This counterstreaming electron event is classified as type 1, because energetic electron fluxes above 1 keV were simultaneously detected.

Ion fluxes from approximately ten to 100 eV were detected at the same time that counterstreaming electrons were observed (see the bottom panel of Figure 14). In conjunction with the enhancement of energetic electron fluxes, the energy of conic ions increased from about 10 eV to about 100 eV. These ion fluxes are identified as conic ions because their pitch angles lay between  $110^\circ$  and  $160^\circ$ . The absence of field-aligned ion fluxes suggests that the observed conic ions are not accelerated by parallel electric fields below the spacecraft.

In Figure 15, we present contours of constant distribution function for a 12-second interval (2147:40-2147:52 UT) during which the counterstreaming electron flux was intense. The contour plots are prepared from a two full spin period of data. The locus of the sampled data in the phase space starts at the upper right corner and is shown as dot. The contours at energies less than 1 keV are elongated along the  $V_{\parallel}$  axis. An island contour at  $V_{\parallel} \approx 9250$  km/s indicates a downward-moving beam at an energy of about 250 eV (positive velocity downward). As in this case, electron beams are sometimes found when counterstreaming electron fluxes are intense. But when counterstreaming electron fluxes are weak, electron beams are generally not observed. Because the plasma data are dominated by spacecraft photoelectrons below 15 eV, we cannot determine whether counterstreaming electrons have a beam energy less than 15 eV.

In Figure 16 we show two consecutive contour plots of constant distribution function that might be considered as representative for counterstreaming electron events. The two contour plots are in time sequence, and each plot is

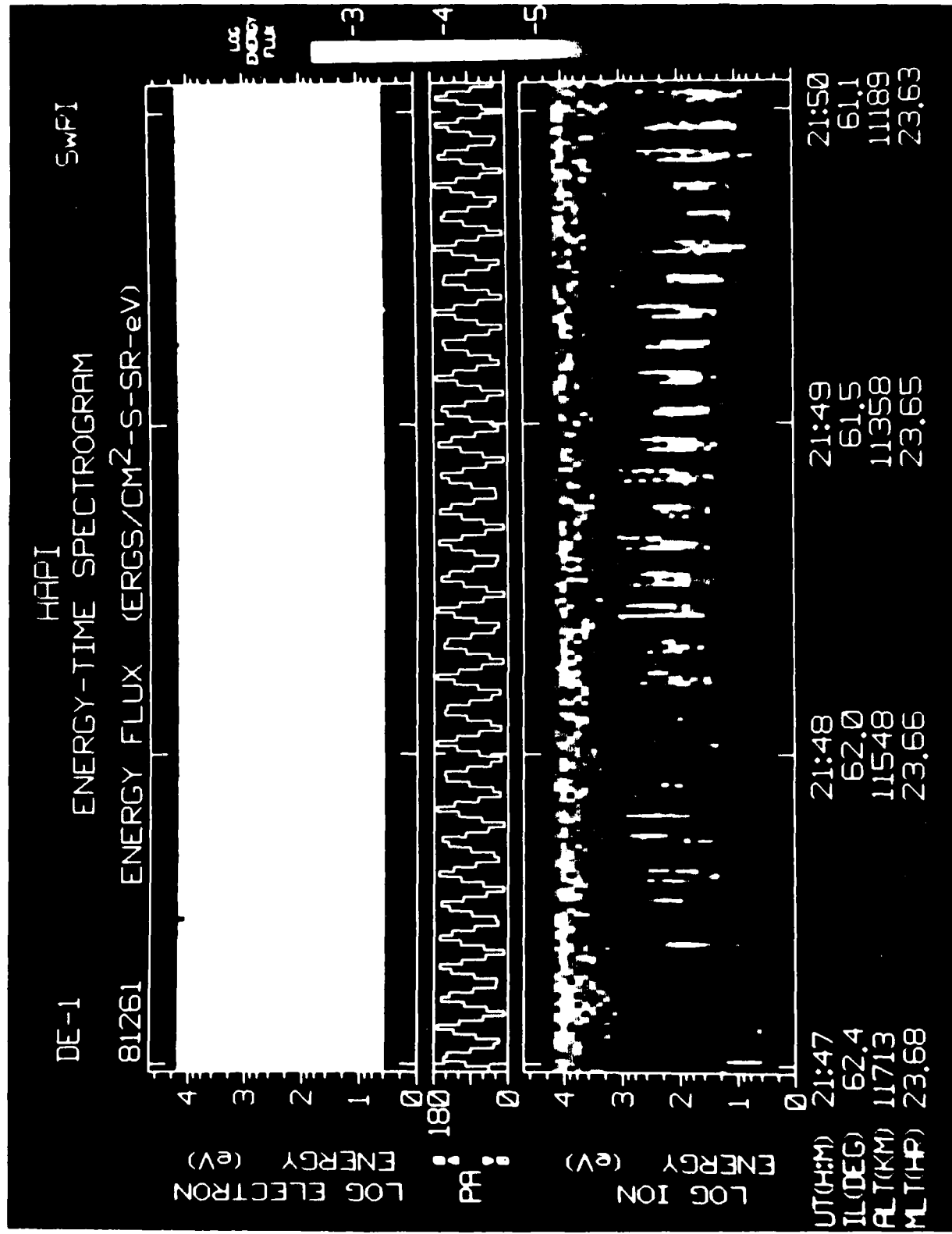
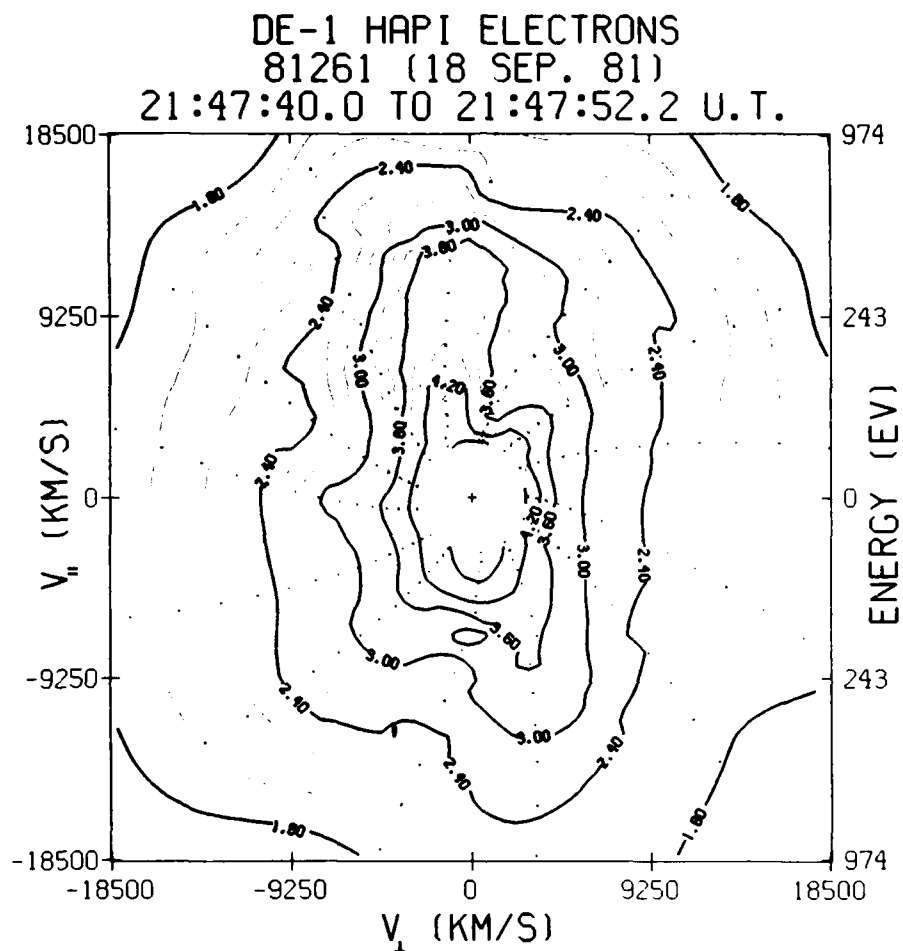


FIGURE 14. Energy time spectrogram of electron (top) and ion (bottom) energy fluxes. The detector's pitch angle is plotted in the center panel.



ILAT (D) 62.2  
MLT (HR) 23.7  
ALT (KM) 11620  
GLAT (D) 40.5  
GLONG (D) 16.3

ILAT (D) 62.1  
MLT (HR) 23.7  
ALT (KM) 11572  
GLAT (D) 40.3  
GLONG (D) 16.2

DISTRIBUTION CONTOURS LOG FISEC<sup>3</sup>/KM<sup>3</sup>

MIN EV	MAX EV	AV. EV.	AMPS/M <sup>2</sup>
6.	9900.	4.12E+02	3.66E-07

FLUX I/CM <sup>2</sup> S	DEN I/CM <sup>3</sup>	ERGS/CM <sup>2</sup> S
0 - 90	0 - 90	0 - 90
1.53E+10	1.98E+01	3.67E+01

VPAR (KM/S)	PC (MMOS)	MC (MMOS)
5.69E+01	N/A	N/A

FIGURE 15. Phase-space density contours of the logarithm of the electron distribution function. A downward electron beam is displayed as a contour island centered on the positive  $V_{\parallel}$  axis.

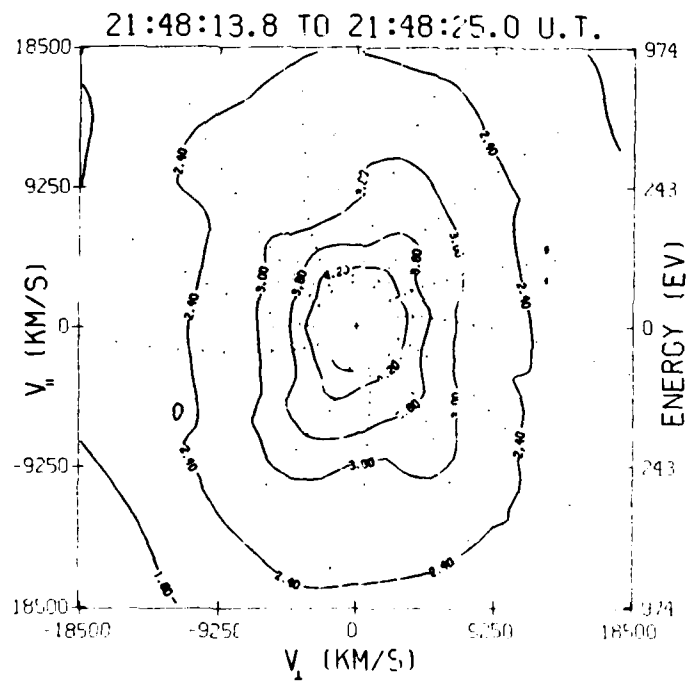
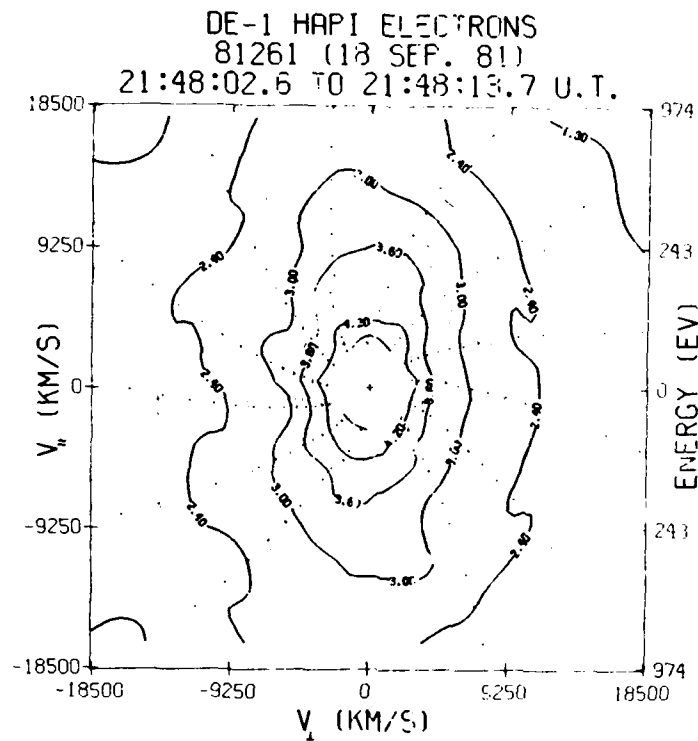


FIGURE 16. Phase-space contours of constant distribution function during a type-I counterstreaming electron event.

composed of the plasma data during a two-spin period. The consistent feature is that the contours are elongated along the  $V_{\parallel}$  axis. Figure 16 differs from Figure 15 in that the contours do not show electron beam. In general, electron beams are found only when counterstreaming electron fluxes are intense. Figure 16 also shows that the contours are less elongated than the contours shown in Figure 15 which covers a time period about 10 seconds earlier. This result suggests that the angular width of field-aligned electron fluxes can vary in time. From the intersections of contours of constant distribution with the two velocity axes, we note that the contours in Figure 16 are slightly more elongated in the direction of positive velocity (toward the ionosphere). From a survey of contour plots, we conclude that the counterstreaming electron fluxes can be slightly enhanced in either upward or downward direction.

The magnetic field measurements during the counterstreaming electron events on day 261, 1981, are shown in Figure 17. The magnetic field instrument was described in detail by Farthing et al., [1981]. The earth's internal field has been subtracted from the observed magnetic field. The residual field components were then transformed into DBR, DBTHETA, and DBPHI in geomagnetic dipole coordinates, where DBR is on the radial direction. DBTHETA is perpendicular to the radius of the meridian plane, and DBPHI points toward the west. The magnetic field data plotted is 1/2-second averaged. The magnetic field disturbance, which was mainly in the DBPHI component, began around 2132 UT.

#### D.2 Magnetic Field Measurements

Figure 12 indicates three counterstreaming electron events occurring in the intervals 2134-2136, 2138-2140 and 2147-2150 UT. Magnetic field perturbations in the azimuthal direction were associated with these three events. During the counterstreaming electron event (2147-2150 UT), DBPHI decreased by 200 nT in 20 seconds starting from 2147:15 UT (Figure 17). This steep decrease of DBPHI represents field-aligned currents flowing into the ionosphere. From 2148 to 2149 UT, DBPHI slowly recovered to its unperturbed value. The energy flux of counterstreaming electrons was most intense (2147:30 -2148 UT) when DBPHI was at its minimum, rather than at its steep gradient.

#### D.3 STARE Measurements

On this pass, DE-1 was magnetically conjugate with STARE. STARE's geographic longitude is 16° east, very close to the DE-1 orbital plane. The STARE

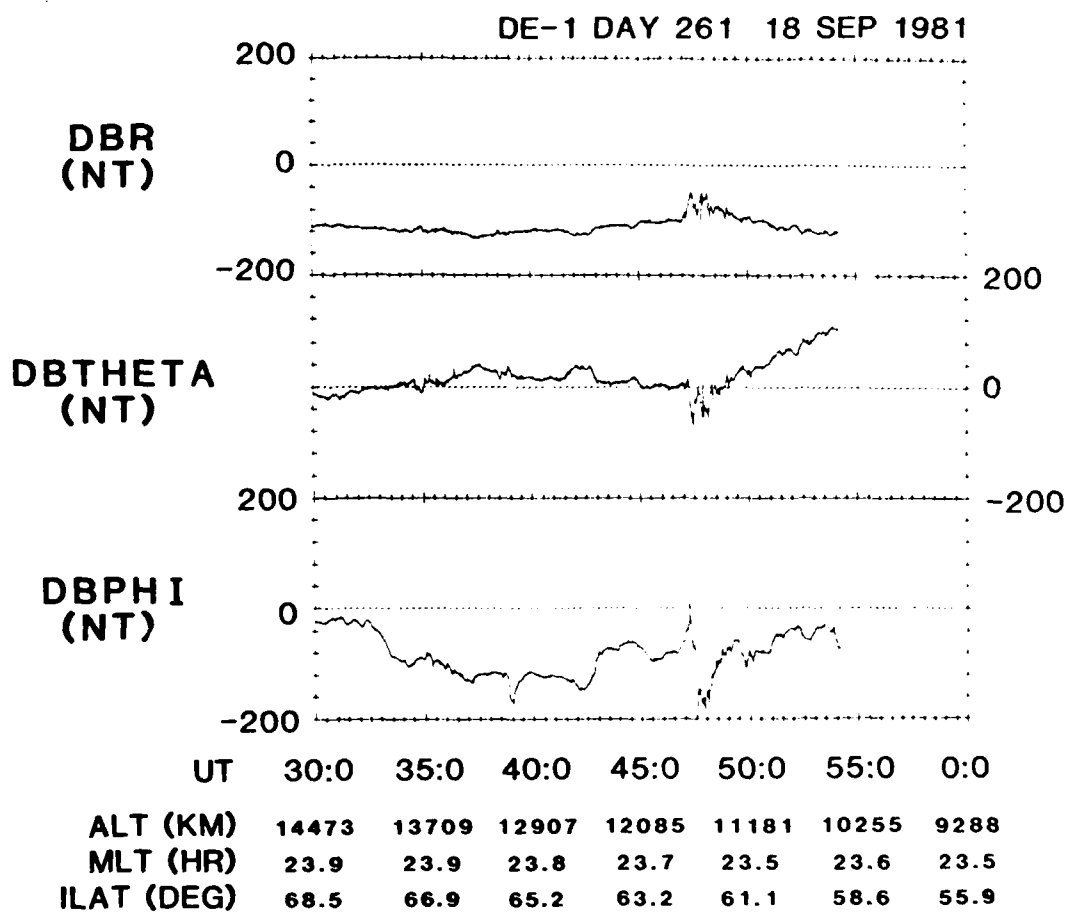


FIGURE 17. Three components of magnetic fields for the DE 1 pass shown in Figure 1.

radars recorded the intensity and Doppler shifts of radio waves scattered by E-layer electron density irregularities [Nielsen and Greenwald, 1979]. By combining the Doppler shifts observed from two separate radars, one then estimates the electron  $\mathbf{E} \times \mathbf{B}$  drift velocity of the E layer irregularities.

Figure 18 illustrates the latitudinal profile of electron drift velocities observed by the STARE system from 2120 to 2143 UT. The electron drift velocities are plotted in a format that has geomagnetic latitude as the vertical coordinate and UT as the horizontal coordinate. Each vector represents a one-minute average of radar measurements. The electron drift velocity started to increase at about 2130 UT in the region equatorward of  $68^\circ$  geomagnetic latitude, about three minutes before the plasma injection boundary was detected by DE-1. Because DE-1 was slightly southward of STARE, this observation can be interpreted by an equatorward motion of the plasma injection boundary. Since most drift vectors were directed eastward, the electric field ( $\mathbf{E} = -\mathbf{V} \times \mathbf{B}$ ) was directed equatorward. This suggests that a Pedersen current was flowing in the equatorward direction. The magnitude of the Pedersen current increased with latitude because the drift velocity increased with latitude. The increase of Pedersen current with latitude suggests an upward field-aligned current flowing in the observation area of STARE after 2130 UT.

The field-aligned current density is estimated from STARE data. Assuming a homogeneous Petersen conductivity of 1 mho, we estimate that the upward field-aligned current density at 2133 UT was about  $0.1 \mu\text{A}/\text{m}^2$ . At 2148 UT, the field-aligned current was upward but flanked by downward currents. The magnitude of field-aligned current density is estimated to be about  $0.4 \mu\text{A}/\text{m}^2$  for a homogeneous Petersen conductivity of 1 mho. Due to uncertainties on the electric field magnitude derived from STARE data, the current density estimates are very rough. However, the directions of field-aligned current deduced from STARE are usually reliable.

#### D.4 Ground Magnetograms

The H-components recorded by five ground magnetograms in the northern auroral zone are shown in Figure 19. These magnetograms indicate that a magnetic substorm started around 1940 UT at the stations in Scandinavia. Near 21 hr UT, all magnetograms recorded active magnetic disturbances. According to



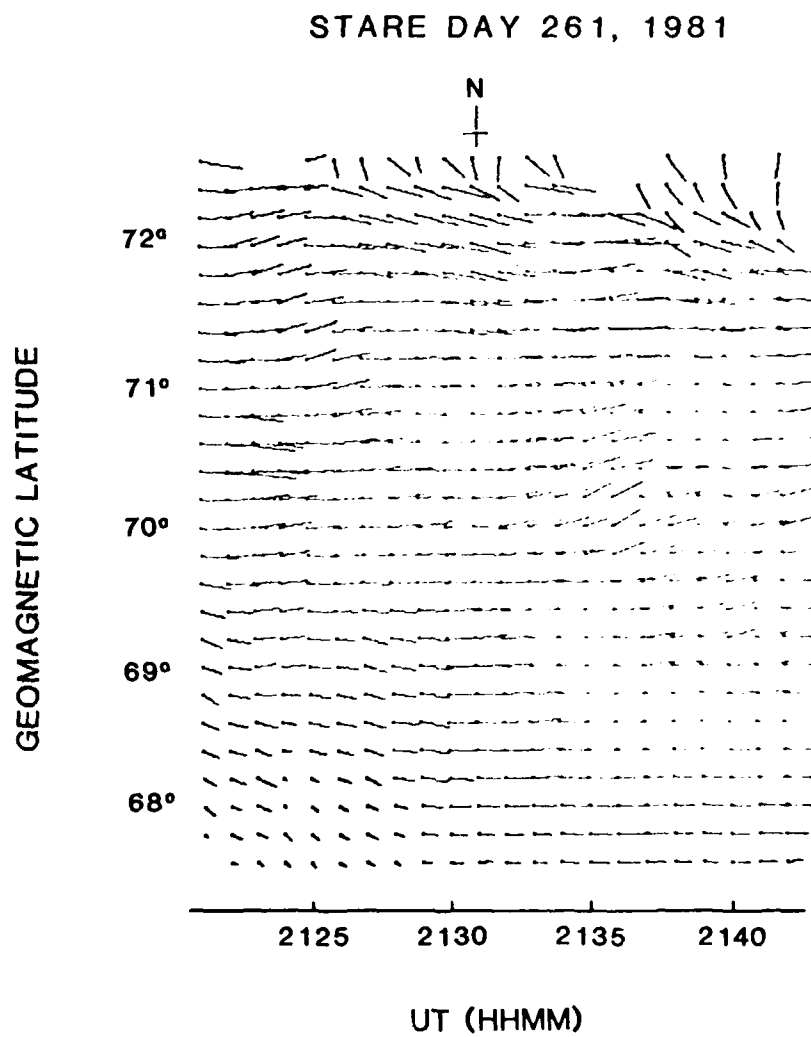


FIGURE 18. STARE latitudinal profile of electron drift velocities versus time on day 261, 1981.



FIGURE 19. Ground magnetograms in the northern auroral zone on 18 September (day 261), 1981.

the Abisko and Tromso stations at about 2° east of the DE-1 orbital plane, the H component began to recover after 2130 UT and returned to its pre-substorm value after 22 hr UT at Tromso and after 23 hr UT at Abisko. We conclude that the plasma injection event observed by DE-1 occurred during the recovery phase of a magnetic substorm.

#### D.5 Computation of Current Density

We compute field-aligned current density from the magnetic field data and from the plasma data. Assuming a series of field-aligned infinite current layers that are locally normal to the dipolar meridian plane, the azimuthal (east-west) component of the magnetic field DBPHI is differentiated to yield the current density. The differentiation of the magnetic field is made with respect to the distance normal to the current sheets. From the measured electron distribution  $f(v, \alpha, \phi)$ , the field-aligned current density is calculated by

$$I = e \int_0^{2\pi} \int_0^\pi \int_{V_{\min}}^{V_{\max}} V_{\parallel} f V_{\perp} dV d\alpha d\phi \quad (1)$$

where  $\alpha$  is pitch angle,  $e$  is electron charge,  $V_{\parallel}$  and  $V_{\perp}$  are the velocities parallel and perpendicular to magnetic field  $B$ ,  $V_{\min}$  and  $V_{\max}$  are the velocity limits on the measurement, and  $\phi$  is the azimuthal angle about  $B$ . We set  $V_{\min}$  equal to the velocity of an 18 eV electron to avoid the spacecraft photoelectrons, and set  $V_{\max}$  equal to the velocity of a 10 keV electron. The time interval to acquire the electron distribution function over the whole pitch angle range is 6 seconds for the normal mode operation of the plasma instrument.

Figure 20 illustrates the current density computed for the interval corresponding to Figure 14. The current density computed from plasma data is given in the top panel and the current density computed from magnetic data is given in the center panel. The azimuthal component of the magnetic field is also presented at the bottom panel for comparison. The plasma data suggest a downward current density with a peak value of  $1.5 \mu\text{A}/\text{m}^2$  occurring at 2147:15 UT. The peak current density derived from the magnetic field data is about  $2 \mu\text{A}/\text{m}^2$ . Integrated over the current layer, the total current densities deduced from both methods are in good agreement and are approximately 0.1 A/m within 10%.

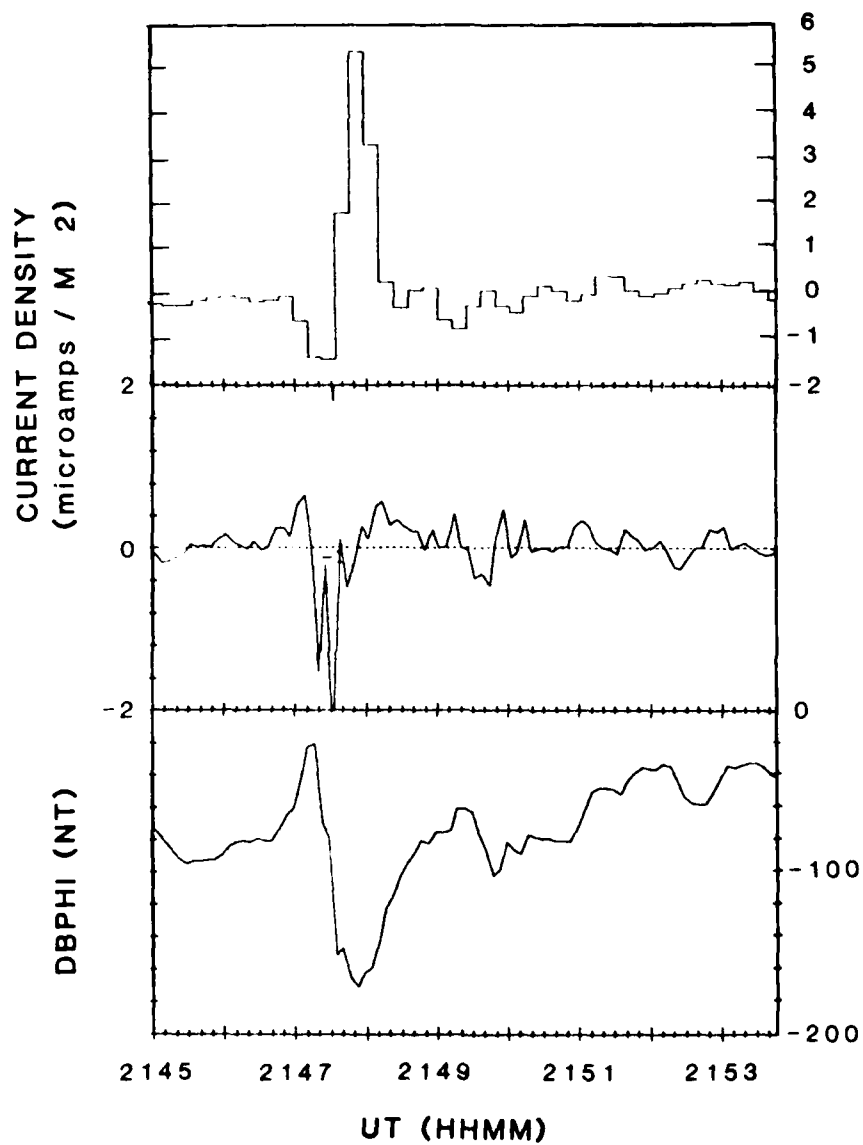


FIGURE 20. Comparison of the current density deduced from the plasma data (top) and the current density deduced from the magnetic field data (center). The bottom panel gives the azimuthal magnetic field component from which the current density was deduced.

The magnetic field data indicate upward currents on both sides of the downward current with a peak current density around  $0.5 \mu\text{A}/\text{m}^2$ . This current density is consistent with the estimate based on the STARE data, but the plasma data suggest a large upward current around 2148 UT with a peak density of about  $5 \mu\text{A}/\text{m}^2$ , about ten times larger than current density computed from the magnetic data. The disagreement could mean that the upward current was a filament or that the upward plasma current was partially neutralized by cold electrons moving in the upward direction.

The contribution of field-aligned current density by counterstreaming electrons was investigated statistically. We surveyed the available DE-1 plasma data that have been processed so far, and found a total of 18 counterstreaming electron events. These events were observed in the evening auroral zone, where their magnetic local times were between 20 and 24 hr, and their invariant latitudes varied from  $60^\circ$  to  $72^\circ$ . These events occurred at altitudes between 9000 km and 14500 km.

We computed differential current density below 235 eV,  $I(<235 \text{ eV})$ , and the total current density,  $I_{\text{total}}$ , from the plasma data. The stepped energy of 235 eV was chosen as the threshold because the energy of counterstreaming electrons is found to be less than 250 eV for most events. The survey of S3-3 data also indicates that 70% of electron beams were detected below 240 eV [Collin et al., 1982]. The largest current density found was  $5 \mu\text{A}/\text{m}^2$  on day 81261 (see Figure 9). Most counterstreaming electron events had a total current density less than  $2 \mu\text{A}/\text{m}^2$ . The total current density was smaller than  $0.25 \mu\text{A}/\text{m}^2$  for only two events. For those events with  $I_{\text{total}}$  greater than  $0.25 \mu\text{A}/\text{m}^2$ , we plot the ratio  $I(<235 \text{ eV})/I_{\text{total}}$  versus  $I_{\text{total}}$  in Figures 21 and 22. For the downward current (open circle),  $I(<235 \text{ eV})$  was greater than 40% of the total current density (Figure 21). For the upward current (solid circle),  $I(<235 \text{ eV})$  was smaller than 50% of the total current density (Figure 22).

#### D.6 Energy and Pitch Angle Distributions

In this section, we examine the properties of electron distribution functions during type 1 counterstreaming electron events. We present line plots of distribution functions with small pitch angles ( $<25^\circ$ ) in the energy range of 20-1000 eV during the interval from 2147:30 to 2149 UT (Figure 23). To the first order approximation, these distribution functions can be presented by

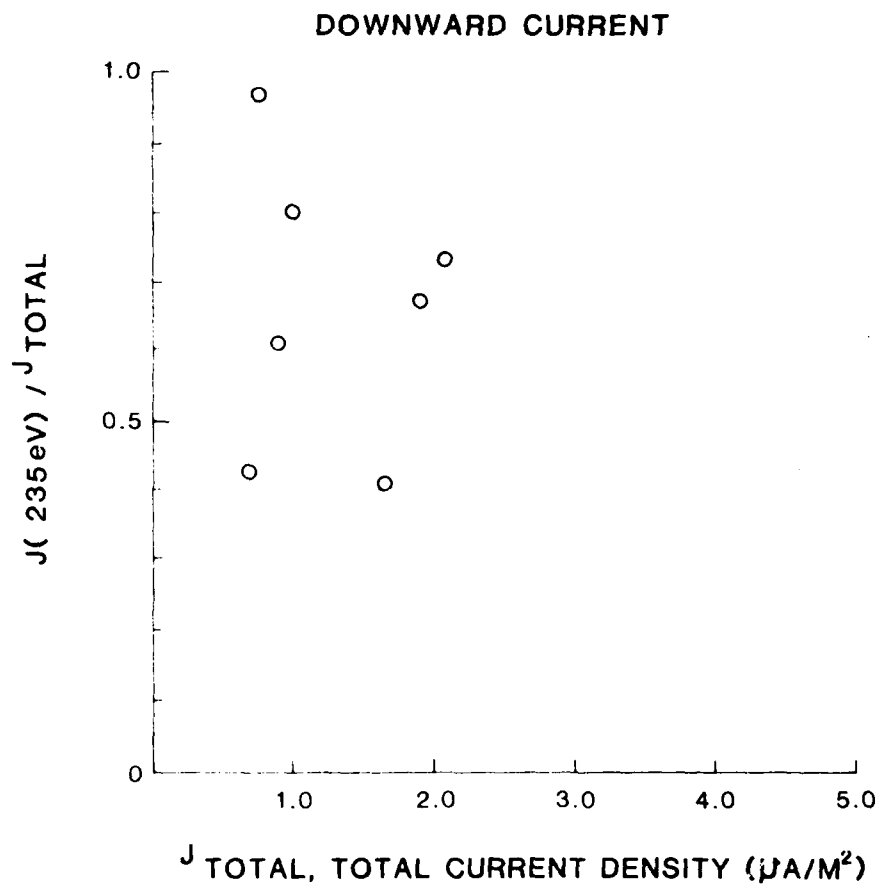


FIGURE 21. Ratio of current densities  $I(<235 \text{ eV})/I_{\text{total}}$  versus  $I_{\text{total}}$  for downward currents. The current density  $I(<235 \text{ eV})$  is integrated from the plasma data from 18 to 10,000 eV.

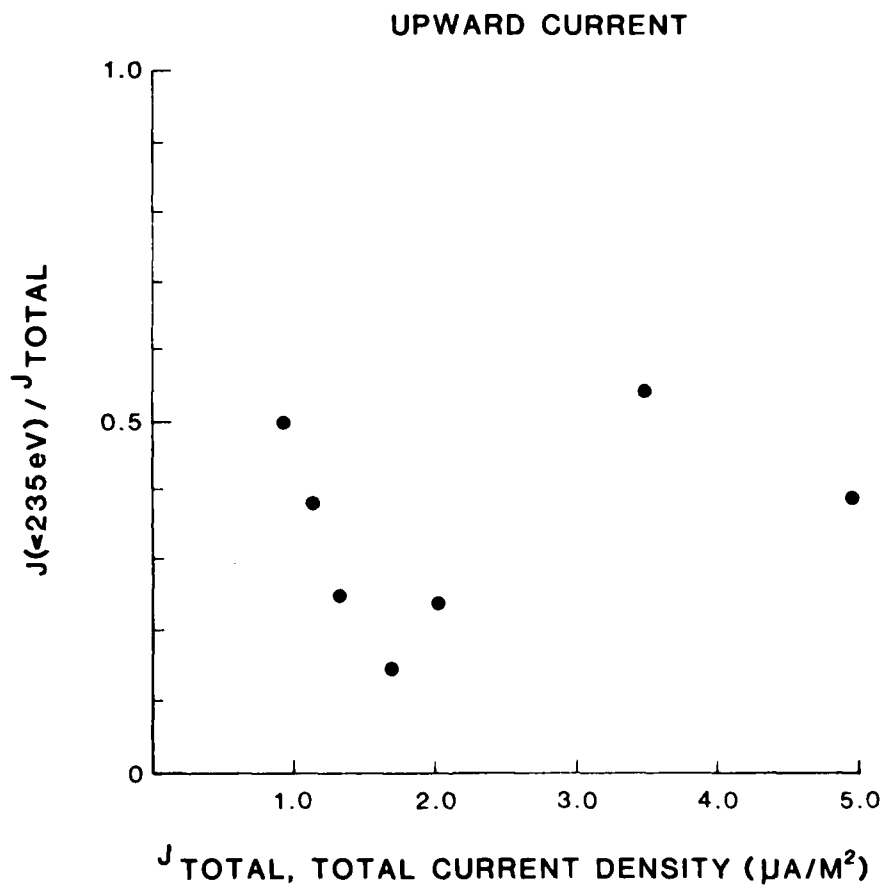


FIGURE 22. Ratio of  $I(<235\text{ eV})/I_{\text{total}}$  versus  $I_{\text{total}}$  for upward currents.

Maxwellian functions, but weak electron beams with energy less than 200 eV were also detected, most distinctly in Figure 23b, c, and g. These electron beams moved in the downward direction and were observed in the region of upward field-aligned currents (Figure 20). The distribution functions for electrons with pitch angles greater than  $155^\circ$  for the interval 2147 -2149 UT are shown in Figure 24. Only two out of the eight distribution functions shown contain weak electron beams with energies around 300 eV (Figure 24b and c). These upward electron beams appeared to be insignificant in determining the direction of field-aligned current because they were detected in the region of upward field-aligned currents (Figure 20).



DATE : 81261  $\alpha < 25^\circ$

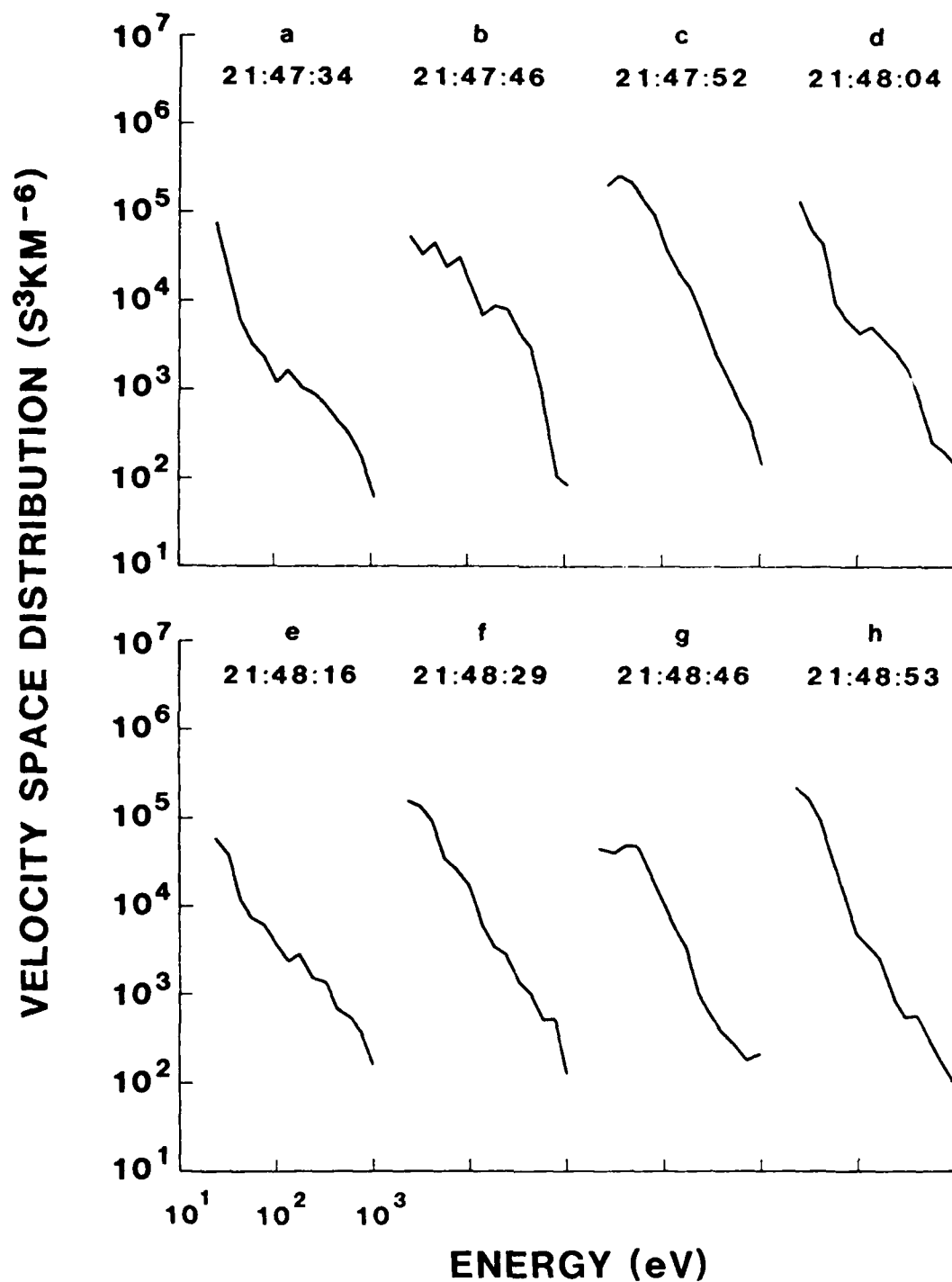


FIGURE 23. Electron distribution functions in the downward field aligned direction.

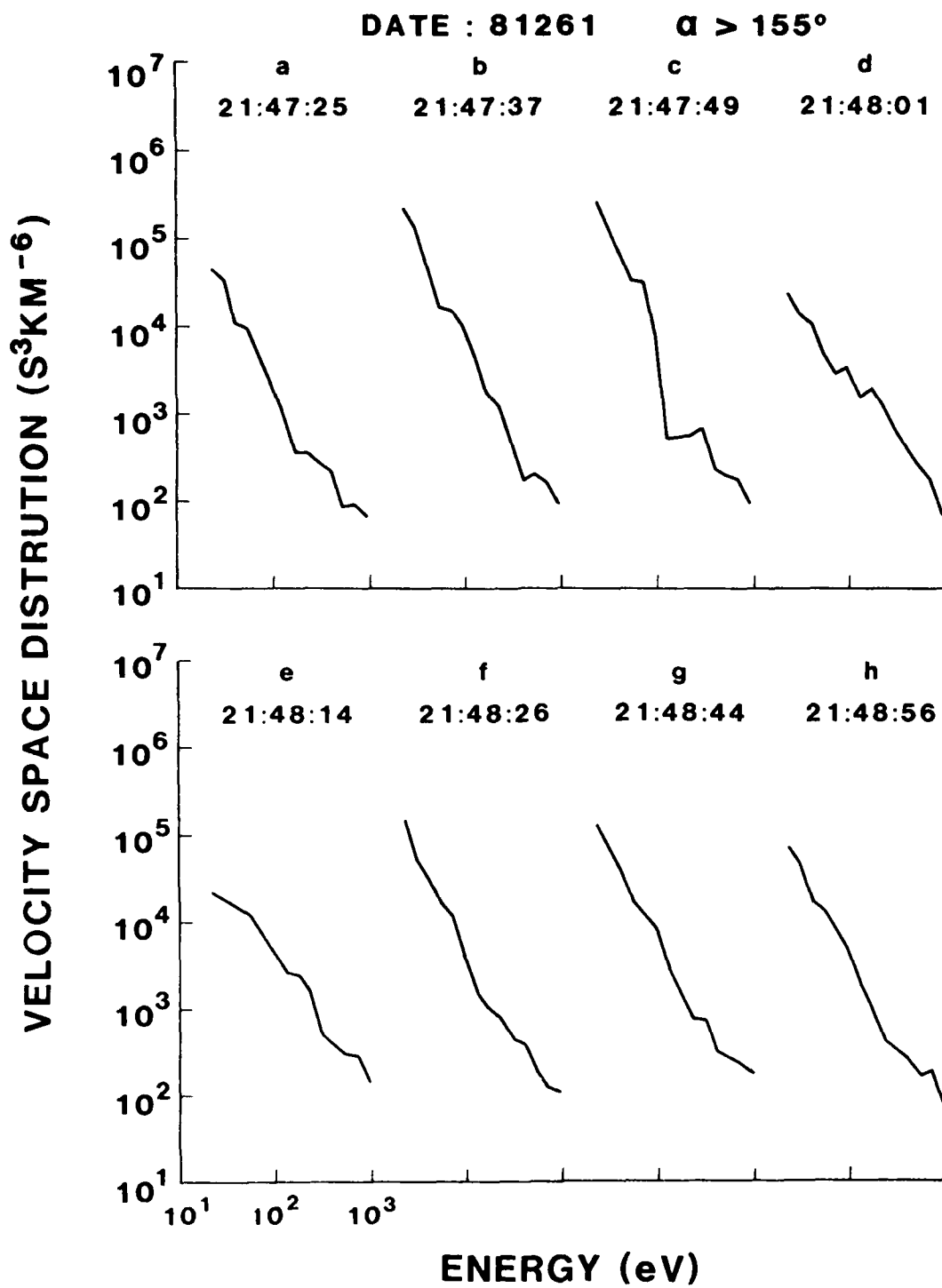


FIGURE 24. Electron distribution functions in the upward field aligned direction

#### IV. PRESENT STATUS AND FUTURE STUDIES

Plasma measurements made on the Dynamics Explorer 1 and 2 spacecraft are providing new information on the altitude dependence of polar-cap plasma populations, their sources, and the acceleration processes they undergo. In this study we have found that the polar-rain electron population apparently exhibits no significant altitude dependence between altitudes of a few hundred to ~20,000 km. This result was expected from the magnetosheath-like energy spectrum of the low-altitude polar rain.

In the case of the polar wind, a significant velocity increase was theoretically predicted to occur between the two spacecraft altitudes, and this effect has been confirmed by the DE-1 plasma measurements. A major result of our study of the accelerated polar wind is its significant conic component, which indicates that the ions are heated perpendicularly as they emerge from the polar-cap ionosphere. The gradual decrease in polar-wind energy that is observed to occur from the cusp across to the nightside polar cap suggests that the perpendicular heating process, probably in cyclotron waves, is most intense near the cusp region.

Significant altitude effects are also observed in the plasmas that occupy magnetic flux tubes connected to polar-cap auroral arcs (or theta auroras). At DE-2, typical low-energy (~100 eV) inverted-V electron distributions are observed. At DE-1 the electron and positive-ion distribution functions are consistent with electrostatic potential drops that are at times below the typical DE-1 altitude of 15,000 to 20,000 km and at times above these altitudes. Thus, compared to auroral-oval acceleration regions those in the polar cap appear to be weaker and at significantly higher altitudes.

The DE-1 observations of plasma and magnetic field during type 1 counterstreaming counterstreaming electron events are summarized as:

1. Counterstreaming electrons are observed at high altitudes ( $>1.5 R_E$ ) in the region of field-aligned current as indicated by the magnetic field data.
2. The total current density computed from the plasma data in the energy range from 18 to 10000 eV is generally about 1-2  $\mu A/m^2$ .

3. For the downward current, low energy ( $18 < E < 235$  eV) electrons contribute more than 40% of the total plasma current density integrated above 18 eV. For the upward current, low energy ( $18 < E < 235$  eV) electrons contribute less than 50% of the total plasma current density integrated above 18 eV.

4. Electron beams in the field-aligned direction are occasionally detected. In general, the pitch angle distributions of counterstreaming electrons are enhanced at both small ( $< 40^\circ$ ) and large ( $> 140^\circ$ ) pitch angles.

5. For one DE-1 pass (on day 261, 1981), STARE simultaneous observations indicated that the field-aligned current was closed through Pedersen currents in the ionosphere. The directions of the ionospheric current systems are consistent with the DE-1 observations at high altitudes.

Collin et al., (1982) have extensively surveyed the occurrence and characteristics of electron beams observed by the S3-3 satellite. They found that the occurrence frequency of counterstreaming electrons increases with altitude in the altitude range examined (3000-8000 km). When including upward, downward, and counterstreaming electron beams, they also found that 85% of electron beams are observed between  $63^\circ$  and  $81^\circ$  invariant latitude and that the magnetic local time distribution is peaked at 7 hr and 22 hr MLT. The number of counterstreaming electron events from the initial survey of DE-1 observations is still limited. But all the events were observed in the evening hours (20-24 hr MLT) and at invariant latitudes between  $60^\circ$  and  $72^\circ$ . For the events observed near magnetic local midnight (on day 261, 1981), the ground magnetograms indicate that these events occurred during the recovery phase of a magnetic substorm. It is apparent that the relationship between counterstreaming electron events and the substorm phenomena remains to be investigated.

The relationship between field-aligned currents and particle precipitation is complicated. The field-aligned current computed from the plasma data is generally correlated with magnetic field perturbations in the azimuthal direction. However, the current density computed from the plasma data does not always agree with the current density modelled from the azimuthal magnetic field perturbation. As has been discussed by Sugiura et al. [1983] with the DE-2 data, the field-aligned currents are electrostatically consistent with the electric field. The current density derived from the plasma data generally do agree with that derived from the magnetic field data in general shape, but with respect to magnitude, these two derivations do not necessarily agree. The difference between these two current densities must be carried by the thermal

plasma so as to achieve the electrodynamic consistency. The disagreement might partially stem from the different methods of computing current density. The magnetic field data used here to deduce the current density are averaged over six seconds, approximately the spin period, to eliminate the spin modulation completely. Therefore, the actual instantaneous current density may be higher than this average. From the plasma data, the current density is numerically integrated above an energy threshold (18 eV in this study). The contribution to the current density from cold electrons might be significant. In computing the current density from the magnetic field data, an infinite current sheet is assumed. As pointed out by Berko et al., (1975), the field-aligned current might be a filament instead of an infinite sheet. These shortcomings are probably the main factors causing the disagreement between the plasma data and the magnetic field data.

One example of such a disagreement is found around 2148 UT on day 261, 1981. The plasma data indicated a large positive current with a density of about 5  $\mu\text{A}/\text{m}^2$ , while the magnetic field data suggested a much smaller current density. We followed the approach of Berko et al., (1975) to examine whether a filament current model might resolve the disagreement. We fitted the observed current densities by Gaussian functions (top, Figure 25). From the fitted current density  $I(r)$ , the azimuthal magnetic field perturbation  $\Delta B_\phi$  is computed with the assumption that the field-aligned current is a cylindrically symmetric filament:

$$\Delta B_\phi = \frac{4\pi}{c} \int_0^R I(r) r dr, \quad (2)$$

where  $R$  is the distance from the observing position to the center of the current filament. Figure 25 shows that the modelled  $\Delta B_\phi$  (dashed curve) does not agree with the observed DBPHI (solid curve). We thus conclude that the filament current model could not resolve the discrepancy in the values of current density from the plasma data and from the magnetic field data.

During this time, the DE-1 plasma wave instrument indicated that the upper hybrid resonance frequency was about 70 kHz. From the observed magnetic field magnitude, we estimate that the electron plasma frequency was about 68 kHz and

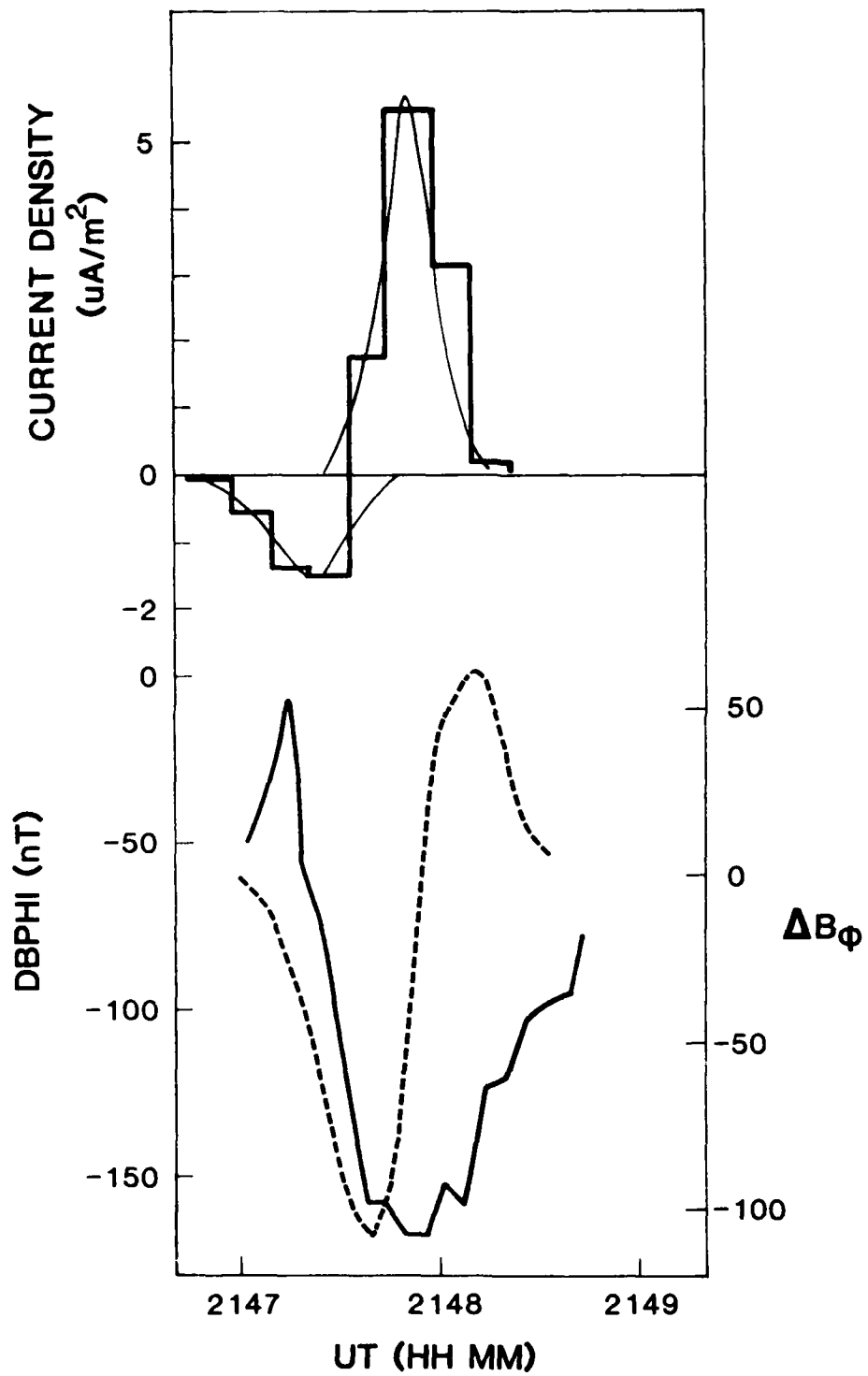


FIGURE 25. Comparison of the observed magnetic field perturbation and the modelled magnetic field perturbation on the assumption that the field aligned current computed from the plasma data was a filament.

the total electron density was about  $57 \text{ cm}^{-3}$ . Because the plasma density integrated above 18 eV was about  $30 \text{ cm}^{-3}$  (Figure 26), we estimate the cold plasma density at energies below 18 eV to be about  $27 \text{ cm}^{-3}$ . The discrepancy in the values of current density computed from the plasma data and from the magnetic field data can be accounted for if cold electrons were moving upward with a mean velocity of about 1150 km/s, corresponding to a mean energy of about 4 eV. Cold electrons at such low energies cannot be detected without ambiguity because the spacecraft secondary electrons might dominate the plasma measurements below 15 eV. However, it seems plausible that the field-aligned current carried by counterstreaming electrons and energetic precipitating electrons was partially cancelled by cold electrons with energies of few eV moving in the opposite direction.

We have examined the contribution of energetic precipitating electron fluxes and counterstreaming electrons to the field-aligned current density at high altitudes. The counterstreaming electron fluxes are found to carry a large portion of current density in the case of downward currents. The energy spectra of counterstreaming electrons are frequently characterized by Maxwellian functions. In contrast, the downward field-aligned current near the dayside cusp is mostly carried by upward electron beams [Burch et al., 1983]. The charge carriers for the downward field-aligned current in the nightside auroral zone are therefore different from those responsible for the dayside cusp downward current. The pitch angle distributions indicate that counterstreaming electrons contribute to field-aligned current density due to the imbalance in the flux enhancement in the upward and downward directions.

During the next year, we will continue research in the areas cited above. In addition, the statistical mapping of high-latitude plasma characteristics and the study of spacecraft charging will continue.

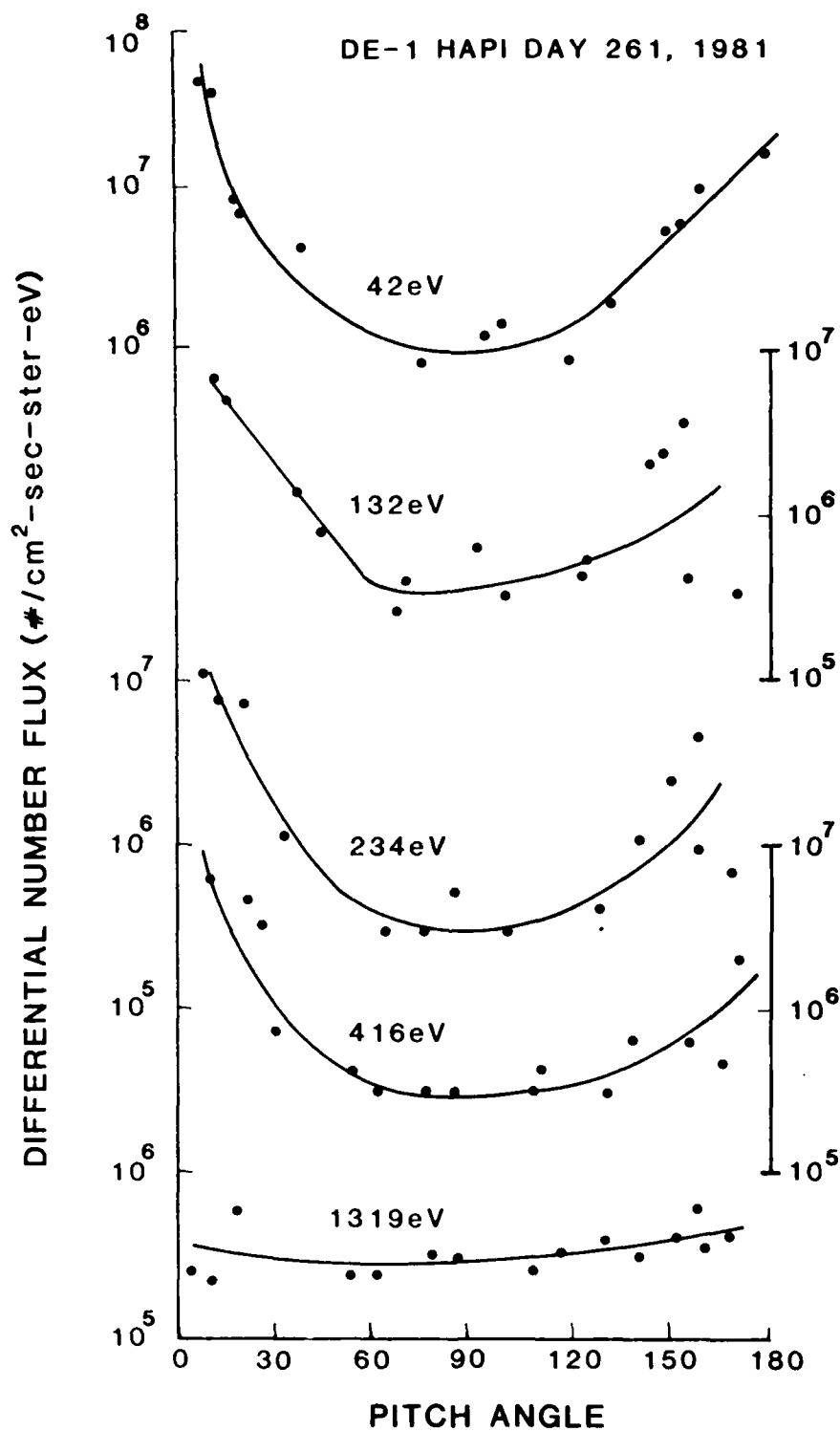


FIGURE 26. Pitch angle distributions at five discrete energies in the interval 2147:41 - 2147:53 UT on day 261, 1981.



# REFERENCES

- Anderson, H. R., and R. R. Vondrak, Observations of Birkeland currents at auroral latitudes, Rev. Geophys. Space Phys., 13, 243, 1975.
- Arnoldy, R. L., Auroral particle precipitation and Birkeland currents, Rev. Geophys. Space Phys., 12, 217, 1974.
- Berko, F. W., R. A. Hoffman, R. K. Burton, and R. E. Holzer, Simultaneous particle and field observations of field-aligned currents, J. Geophys. Res., 80, 37, 1975.
- Burch, J. L., S. A. Fields, and R. A. Heelis, Polar Cap Electron Acceleration Regions, J. Geophys. Res., 84, 5863, 1979.
- Burch, J. L., J. D. Winningham, V. A. Blevins, N. Eaker, W. C. Gibson, and R. A. Hoffman, High-altitude plasma instrument for Dynamics Explorer-A, Space Sci. Instru., 5, 455, 1981.
- Burch, J. L., P. H. Reiff, and M. Sugiura, Upward electron beams measured by DE-1: A primary source of dayside region-1 Birkeland currents, Geophys. Res. Lett., 10, 753, 1983.
- Burke, W. J., D. A. Hardy, F. J. Rich, M. C. Kelley, M. Smiddy, B. Shuman, R. C. Sagalyn, R. P. Vancour, P. J. Widman, and S. T. Lai, Electrodynamic structure of the late evening sector of the auroral zone, J. Geophys. Res., 85, 1179, 1980.
- Burke, W. J., Magnetosphere-Ionosphere Coupling, Contributions from IMS Satellite Observations, Rev. Geophys. Space Phys., 20, 685, 1982.
- Burke, W. J., M. S. Gussenhoven, M. C. Kelley, D. A. Hardy, and F. J. Rich, Electric and Magnetic Field Characteristics of Discrete Arcs in the Polar Cap, J. Geophys. Res., 87, 2431, 1982.
- Chang, T., and B. Coppi, Lower Hybrid Acceleration and Ion Evolution in the Supraauroral Region, Geophys. Res. Lett., 18, 1253, 1981.

- Collin, H. L., R. D. Sharp, and E. G. Shelley, The occurrence and characteristics of electron beams over the polar regions, J. Geophys. Res., 87, 7504, 1982.
- Dusenberry, P. B., and L. R. Lyons, Generation of Ion-Conic Distribution by Upgoing Ionospheric Electrons, J. Geophys. Lett., 18, 1253, 1981.
- Farthing, W. H., M. Sugiura, B. G. Ledley, and L. J. Cahill, Jr., Magnetic field observations on DE-A and -B, Space Sci. Instr., 5, 551, 1981.
- Foster, J. D. and J. R. Burrows, Electron Fluxes over the Polar Cap 1. Intense keV Fluxes During Poststorm Quieting, J. Geophys. Res., 81, 6016, 1976.
- Gorney, D. J., A. Clarke, D. R. Croley, J. F. Fennell, J. Luhman, and P. Mizera, The Distributions of Ion Beams and Conics below 8000 km, J. Geophys. Res., 86, 83, 1981.
- Gurgiolo, C. and J. L. Burch, DE-1 Observations of the Polar Wind--A Heated and an Unheated Component, Geophys. Res. Lett., 9, 945, 1982.
- Hardy, D. A., W. J. Burke, and M. S. Gussenhoven, DMSP Optical and Electron Measurements in the Vicinity of Polar Cap Arcs, J. Geophys. Res., 87, 2413, 1982.
- Hoffman, J. H. and W. H. Dodson, Light Ion Concentrations and Fluxes in the Polar Regions during Magnetically Quiet Times, J. Geophys. Res., 85, 626, 1980.
- Klumpp, D. M., Relationship between auroral particle distributions and magnetic field perturbations associated with field-aligned currents, J. Geophys. Res., 84, 6524, 1979.
- Lin, C. S., B. Mauk, G. K. Parks, S. DeForest, and C. E. McIlwain, Temperature characteristics of electron beams and ambient particles, J. Geophys. Res., 84, 2651, 1979.

- Lin, C. S., J. L. Burch, J. D. Winningham, J. D. Menietti, and R. A. Hoffman, DE-1 observations of counterstreaming electrons at high altitudes, Geophys. Res. Lett., 9, 925, 1982.
- Lysak, R. L., M. K. Hudson, and M. Temerin, Ion Heating by Strong Electrostatic Ion Cyclotron Turbulence, J. Geophys. Res., 85, 678, 1980.
- Moore, T. E., and R. L. Arnoldy, Plasma pitch angle distributions near the substorm injection front, J. Geophys. Res., 87, 265, 1982.
- Nielsen, E., and R. A. Greenwald, Electron flow and visual aurora at the Lang Discontinuity, J. Geophys. Res., 84, 4189, 1979.
- Saflekos, N. A., R. E. Sheehan, and R. L. Carovillano, Global nature of field-aligned currents and their relation to auroral phenomena, Rev. of Geophys. and Space Phys., 20, 709, 1982.
- Schunk, R. D., and D. S. Watkins, Proton Temperature Anisotropy in the Polar Wind, J. Geophys. Res., 87, 171, 1982.
- Senior, C., R. M. Robinson, and T. A. Potemra, Relationship between field-aligned currents, diffuse auroral precipitation and the westward electrojet in the early morning sector, J. Geophys. Res., 87, 10469, 1982.
- Sharp, R. D., E. G. Shelley, R. G. Johnson, and A. G. Ghielmetti, Counterstreaming electron beams at altitudes of  $\sim 1 R_E$  over the auroral zone, J. Geophys. Res., 85, 92, 1980.
- Sugiura, M., N. C. Maynard, W. H. Farthing, J. P. Heppner, and B. G. Ledley, Initial results on the correlation between the magnetic and electric fields observed from the DE-2 satellite in the field-aligned current regions, Geophys. Res. Lett., 9, 985, 1982.
- Sugiura, M., T. Iyemori, R. A. Hoffman, N. C. Maynard, J. L. Burch, and J. D. Winningham, Relationships between field-aligned currents, electric fields, and particle precipitation as observed by Dynamics Explorer-2, Magnetospheric Currents, ed. T. A. Potemra, page 96, AGU, Washington, D. C., 1983.

- Ungstrup, E., D. M. Klumpar, and W. J. Heikkila, Heating of Ions to Super-thermal Energies in the Topside Ionosphere by Electrostatic Ion Cyclotron Waves, J. Geophys. Res., 84, 4289, 1979.
- Winningham, J. D., and W. J. Heikkila, Polar Cap Electron Fluxes Observed with ISIS-1, J. Geophys. Res., 79, 949, 1974.
- Winningham, J. D., F. Yaschara, S. I. Akasofu, and W. J. Heikkila, The latitudinal morphology of 10-eV to 10-keV electron fluxes during magnetically quiet and disturbed times in the 2100-0300 MLT sector, J. Geophys. Res., 80, 3148, 1975.
- Winningham, J. E., J. L. Burch, N. Eaker, V. A. Blevins, and R. A. Hoffman, The Low Altitude Plasma Instrument (LAPI), Space Sci. Instr., 5, 465, 1981.

PAPERS PRESENTED AT SCIENTIFIC MEETINGS

Barfield, J. N., C. S. Lin, J. L. Burch, J. D. Winningham, C. Gurgiolo, J. D. Menietti, and N. A. Saflekos, Polar Plasmas as Observed by Dynamics Explorer 1 and 2, paper presented at USAF/NASA Spacecraft Environmental Interactions Technology Conference, October, 1983.

PUBLICATIONS SUPPORTED BY CONTRACT

Lin, C. S., M. Sugiura, J. L. Burch, J. N. Barfield, and E. Nielsen, DE-1  
Observations of Type-1 Counterstreaming Electrons and Field-Aligned  
Currents, accepted by Journal of Geophysical Research, 1984.

# PERSONNEL

The following persons contributed to the work reported.

J. N. Barfield, principal investigator  
C. S. Lin  
J. L. Burch  
J. D. Winningham  
C. Gurgiolo  
J. D. Menietti  
R. W. Janetzke  
L. Garcia  
K. Elizondo  
K. Birkelbach

**END**

**FILMED**

**10-84**

**DTIC**